AD-A037 523 CALIFORNIA UNIV LOS ANGELES DEPT OF PHYSICS F/G 20/9
COUPLING OF LOWER-HYBRID RADIATION AT THE PLASMA EDGE.(U)
JAN 77 G J MORALES N00014-75-C-0476
UNCLASSIFIED PPG-288 NL

1 OF 1
ADA037523

END

DATE FILMED
4-77

SECURITY CLASSIFICATION OF THIS PAGE *(When Data Entered)*

REPORT DOCUMENTATION PAGE	READ INSTRUCTIONS BEFORE COMPLETING FORM
1. REPORT NUMBER (14) PPG-288 — 2. GOVT ACCESSION NO.	3. RECIPIENT'S CATALOG NUMBER
4. TITLE *(and Subtitle)* (6) Coupling of Lower-hybrid Radiation at the Plasma Edge. (10) P.S.	5. TYPE OF REPORT & PERIOD COVERED (9) Technical rept.
	6. PERFORMING ORG. REPORT NUMBER
7. AUTHOR(s) (10) G. J. Morales	8. CONTRACT OR GRANT NUMBER(s) ONR N00014-75-C-0476 P00002 (15)
9. PERFORMING ORGANIZATION NAME AND ADDRESS Department of Physics University of California Los Angeles, California 90024	10. PROGRAM ELEMENT, PROJECT, TASK AREA & WORK UNIT NUMBERS NR-012-306
11. CONTROLLING OFFICE NAME AND ADDRESS Office of Naval Research Physics Program Office Arlington, Virginia 22217 (11)	12. REPORT DATE January 1977 13. NUMBER OF PAGES 56 pages
14. MONITORING AGENCY NAME & ADDRESS *(if different from Controlling Office)* (12) 58 p.	15. SECURITY CLASS. *(of this report)* Unclassified 15a. DECLASSIFICATION/DOWNGRADING SCHEDULE Unclassified

16. DISTRIBUTION STATEMENT *(of this Report)*

Approved for public release: distribution unlimited

17. DISTRIBUTION STATEMENT *(of the abstract entered in Block 20, if different from Report)*

18. SUPPLEMENTARY NOTES

To be published in Physics of Fluids

19. KEY WORDS *(Continue on reverse side if necessary and identify by block number)*

Plasma heating, Nonlinear profile modifications.

20. ABSTRACT *(Continue on reverse side if necessary and identify by block number)*

See attached sheet

DD FORM 1 JAN 73 1473 EDITION OF 1 NOV 65 IS OBSOLETE
S/N 0102-LF-014-6601

SECURITY CLASSIFICATION OF THIS PAGE *(When Data Entered)*

072 267

Abstract

This investigation considers the mode-conversion process encountered in the lower-hybrid heating scheme at the edge of the plasma, where the frequency of the external radiation is comparable to the local value of the electron plasma frequency. The problem is formulated in terms of a modulational representation of the electric field that permits the description of the full space-time evolution of the process. The numerical study of the model equations confirm that a backward wave is excited at the edge and that it leads to a net energy flow directed toward the interior of the plasma. For small external power levels, the flow is characterized by the propagation of a leading-edge pulse whose arrival at a given spatial location marks the onset of the steady-state. At large external power levels, the self-consistent modification of the density profile by the ponderomotive force is found to quench the mode-conversion process, thus causing a significant reduction in the amount of RF energy that can be coupled from the external source to the interior of the plasma.

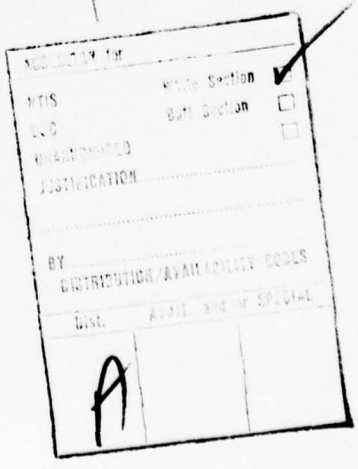

COUPLING OF LOWER-HYBRID RADIATION AT THE PLASMA EDGE

G. J. Morales

PPG-288 January 1977

Department of Physics
University of California
Los Angeles, California 90024

Abstract

This investigation considers the mode-conversion process encountered in the lower-hybrid heating scheme at the edge of the plasma, where the frequency of the external radiation is comparable to the local value of the electron plasma frequency. The problem is formulated in terms of a modulational representation of the electric field that permits the description of the full space-time evolution of the process. The numerical study of the model equations confirm that a backward wave is excited at the edge and that it leads to a net energy flow directed toward the interior of the plasma. For small external power levels, the flow is characterized by the propagation of a leading-edge pulse whose arrival at a given spatial location marks the onset of the steady-state. At large external power levels, the self-consistent modification of the density profile by the ponderomotive force is found to quench the mode-conversion process, thus causing a significant reduction in the amount of RF energy that can be coupled from the external source to the interior of the plasma.

I. Introduction

The goal of an auxiliary plasma heating scheme aimed at achieving thermonuclear temperatures (> 10 KeV) consists of delivering a large amount of external energy to the interior of a pre-existing plasma having a moderate initial temperature (< 3 KeV). The various auxiliary heating schemes being considered at the present time differ mainly in the form of the primary energy used, e.g., the neutral-beam heating approach uses the streaming or kinetic energy of the injected particles, while the RF heating schemes utilize electromagnetic energy directly.

Regardless of the particular heating method considered, in its implementation phase one always encounters the following major physics questions: 1) How is the external energy transferred to the ions once it reaches the interior of the plasma?, 2) How is the external energy transported from the edge of the plasma to the interior?, and 3) How does the external source couple to the surface of the plasma? It should be noted that the existence of potentially deleterious answers to any of these questions may render the entire heating scheme inapplicable as far as the attainment of fusion conditions is concerned, even though the scheme may be quite meritorious on the grounds of the existence of a well-developed technology or because of its ease of implementation.

Historically, it has been the case that the interest of the plasma physics community has been focused mainly on the issues surrounding question 1) and only peripherally on those matters pertaining to questions 2) and 3). However, with the ever increasing need to assess the future potential of auxiliary heating schemes it becomes important to consider the fundamental physics of processes that may be encountered in answering questions

2) and 3). It is in this general direction that the present investigation is aimed. Specifically, this study isolates some of the surface-coupling properties of external electromagnetic radiation in the lower-hybrid frequency range.

The particular case which pertains to the present investigation is the lower-hybrid heating scheme proposed by Stix[1] over a decade ago. A large fraction of the theoretical effort in this topic has been devoted to elucidating the numerous processes which may occur deep in the interior of the plasma, where the frequency of the external radiation, ω, matches the peak value of the lower-hybrid frequency $\omega_{LH} = \omega_{pi}/[1 + (\omega_{pe}/\Omega_e)^2]^{\frac{1}{2}}$, in which ω_{pe} and ω_{pi} refer to the electron and ion plasma frequencies, and Ω_e represents the electron gyrofrequency.

Over the past year, it has become increasingly evident that major difficulties may be encountered in this heating scheme in the process of transporting the RF energy from the edge of the plasma to the interior, i.e., before the condition $\omega = \omega_{LH}$ is ever attained. Numerous theoretical studies of parametric instabilities[2-4], of lower-hybrid cone filamentation[5,6], as well as explicit experimental measurements[7] of filamentation phenomena and associated plasma heating in small-scale experiments, have contributed to the general realization of this point of view. Yet, a more direct and compelling argument has been provided by the results of the large-scale lower-hybrid heating experiments performed in Alcator[8] at MIT, and in the ATC tokamak at Princeton[9].

Although the details of the outcome of these experiments are difficult to interpret, it is important to recognize that both of these studies are consistent with the view that the external RF energy is efficiently injected

from the source waveguide into the plasma-filled vacuum vessel, and thereafter it propagates in the vicinity of the plasma edge, with only a relatively small fraction of the injected energy penetrating to the interior. Therefore, it is of interest to isolate some of the basic processes which may play a role in the coupling of external RF energy in the lower-hybrid frequency range at the edge of a plasma.

The present study is concerned explicitly with the mode-conversion process which is encountered in the low density region at the edge of the plasma where the frequency of the incoming radiation is of the order of the local electron plasma frequency, i.e., $\omega \sim \omega_{pe}$. To simplify the problem a slab model is considered in which the density varies in the direction perpendicular to the external magnetic field. Unlike previous studies of the mode-conversion process [10,11], which have dealt exclusively with the steady-state properties, the present formulation uses a modulational representation for the electric field which permits the description of the full space-time evolution of the detailed process.

The numerical study of the relevant model equations of the problem demonstrate that in the region where $\omega_{pe} > \omega$ a backward wave is excited and leads to the propagation of RF energy away from the plasma edge toward the interior. An interesting feature of this transport is the existence of a propagating leading-edge pulse whose arrival at a given spatial location marks the onset of the steady-state pattern.

The present formulation also permits the study of more complicated non-

linear processes which may take place at the plasma edge when large external power levels are applied. In particular, the present study has considered the effects produced by the profile modification caused by the ponderomotive force associated with the intense electric fields. It is found that this effect can alter the mode-conversion process to a large degree, thus leading to significant reduction in the penetration of the external RF energy into the plasma.

The manuscript is organized as follows: Sec. II presents the formulation of the problem, its properties, and associated conservation laws. Sec. III discusses briefly the boundary conditions and numerical scheme used to study the model equations. Sec. IV presents the results of the time evolution of mode-conversion in both the linear and nonlinear regimes. A summary of the results obtained is presented in Sec. V.

II. Formulation

To simplify the geometry of the present problem we consider explicitly a plasma slab whose zero-order density $n_o(x)$ increases along the x-direction, which is taken to be perpendicular to the external magnetic field $\underset{\sim}{B}_o$, as is illustrated in Fig. 1. The z-axis of the cartessian coordinate system points along $\underset{\sim}{B}_o$, while the y-axis is perpendicular to the x-z plane, and constitutes the ignorable coordinate of the problem, i.e., there are no explicit functional dependences on it. The total electric field $\underset{\sim}{\mathcal{E}}$ is expressed in the form

$$\underset{\sim}{\mathcal{E}}(x,z,t) = \underset{\sim}{E}(x,t)e^{i(kz - \omega t)} + c.c. \qquad (1)$$

In Eq. (1) k represents the wavenumber along the z coordinate and is assumed to be fixed, physically, by a suitably designed external slow-wave structure or simulated by a properly-phased waveguide array (grill). The fundamental role played by such external devices is that they permit the experimenter to choose the proper value of k that optimizes the penetration of radiation into the plasma. In particular, these devices permit the generation of radiation such that $k > k_o = \omega/c$, where c is the speed of light, and thus k_o represents the vacuum wavenumber. As is well known[1,10,11] this prerequisite must be met by the external radiation in order to satisfy the lower-hybrid accessibility criterion.

In the context of the present problem ω is equal or comparable to the value of the peak lower-hybrid frequency of the plasma; such a value is, of course, attained deep in its interior. In contrast, the region of interest to the present calculation is that where ω is comparable to or within an order of magnitude smaller than the local value of the electron plasma frequency, i.e.,

$$\omega \simeq (\omega_{LH})_{peak} \sim (\omega_{pi})_{peak} \tag{2}$$

thus, the region of interest is defined, for a given density profile, by

$$\omega \lesssim \omega_{pe}(x) \lesssim 10\omega \tag{3}$$

Maxwell's equations for the radiation fields $\underset{\sim}{\mathcal{E}}$ and $\underset{\sim}{B}$ are

$$\begin{aligned} \nabla \times \underset{\sim}{\mathcal{E}} &= -\frac{1}{c}\frac{\partial}{\partial t}\underset{\sim}{B} \\ \nabla \times \underset{\sim}{B} &= \frac{4\pi}{c}\underset{\sim}{j} + \frac{1}{c}\frac{\partial}{\partial t}\underset{\sim}{\mathcal{E}} \end{aligned} \tag{4}$$

which can be combined to yield

$$\nabla \times \nabla \times \underset{\sim}{\mathcal{E}} = -\frac{4\pi}{c^2}\frac{\partial}{\partial t}\underset{\sim}{j} - \frac{1}{c^2}\frac{\partial^2}{\partial t^2}\underset{\sim}{\mathcal{E}} \tag{5}$$

considering Eq. (1) and making use of the modulational approximation (i.e., neglecting the $\partial^2 E/\partial t^2$ term) reduces Eq. (5) to

$$\nabla \times \nabla \times \underset{\sim}{E} = -\frac{4\pi}{c^2} e^{i\omega t}\frac{\partial}{\partial t}\underset{\sim}{j} - k_o^2\underset{\sim}{E} + 2i\frac{k_0^2}{\omega}\frac{\partial}{\partial t}\underset{\sim}{E} \tag{6}$$

In the spirit of the modulational representation we take the self-consistent RF current in the plasma, $\underset{\sim}{j}$, to be determined by the instantaneous value of the electric field, i.e., we neglect time-history contributions to the linear dielectrics. Accordingly,

$$\frac{4\pi}{\omega^2} e^{i\omega t}\frac{\partial}{\partial t}\underset{\sim}{j} + \underset{\sim}{E} \simeq -\overleftrightarrow{\varepsilon} \cdot \underset{\sim}{E} \tag{7}$$

where, $\overleftrightarrow{\varepsilon}$ is the cold plasma dielectric tensor having the form

$$\overleftrightarrow{\varepsilon} = \begin{pmatrix} \varepsilon_{xx} & \varepsilon_{xy} & 0 \\ \varepsilon_{yx} & \varepsilon_{yy} & 0 \\ 0 & 0 & \varepsilon_{zz} \end{pmatrix} \tag{8}$$

The ordering of frequencies in the lower-hybrid scheme is such that $\Omega_i << \omega << \Omega_e$, thus the components of $\overleftrightarrow{\varepsilon}$ are

$$\begin{aligned} \varepsilon_{xx} &= \varepsilon_{yy} \simeq 1 + \left(\frac{\omega_{pe}}{\Omega_e}\right)^2 - \left(\frac{\omega_{pi}}{\omega}\right)^2 \\ \varepsilon_{xy} &= -\varepsilon_{yx} \simeq i\left(\frac{\omega_{pe}^2}{\omega\Omega_e}\right) \\ \varepsilon_{zz} &= 1 - \left(\frac{\omega_{pe}}{\omega}\right)^2 \end{aligned} \tag{9}$$

Using Eq. (7) in Eq. (6) yields

$$\frac{2i}{\omega}\frac{\partial}{\partial t}\underset{\sim}{E} + \overleftrightarrow{\varepsilon}\cdot\underset{\sim}{E} = \frac{1}{k_o^2}\nabla\times\nabla\times\underset{\sim}{E} \tag{10}$$

Writing out explicity the $\nabla \times \nabla$ operator in Eq. (10) produces the following coupled partial differential equations for the components of the electric field

$$\frac{2i}{\omega}\frac{\partial}{\partial t}E_y + \frac{1}{k_o^2}\frac{\partial^2}{\partial x^2}E_y + \left[\varepsilon_{yy} - \left(\frac{k}{k_o}\right)^2\right]E_y = -\varepsilon_{xy}E_x \tag{11}$$

$$\frac{2i}{\omega}\frac{\partial}{\partial t}E_z + \frac{1}{k_o^2}\frac{\partial^2}{\partial x^2}E_z + \varepsilon_{zz}E_z = i\frac{k}{k_o^2}\frac{\partial}{\partial x}E_x \tag{12}$$

$$\frac{2i}{\omega}\frac{\partial}{\partial t}E_x + \left[\varepsilon_{xx} - \left(\frac{k}{k_o}\right)^2\right]E_x = i\frac{k}{k_o^2}\frac{\partial}{\partial x}E_z + \varepsilon_{xy}E_x \tag{13}$$

One envisions the external radiation arriving at the edge of the plasma slab with finite values of E_x and E_z, and with $E_y = 0$. Although not present in the incident radiation, an E_y component develops inside the plasma due to the self-consistent $\underset{\sim}{E} \times \underset{\sim}{B}_o$ currents. However, the generation of this component is rather weak in the region of interest here because, as is seen from Eqs. (9) and (11), the coupling is of order $\omega_{pe}^2(x)/\omega\Omega_e \sim \omega_{LH}/\Omega_e << 1$. Accordingly, the equations governing the space-time evolution of the coupling at the edge of the plasma are of the form

$$i\,\partial_\tau E_z + \partial_\xi^2 E_z + \varepsilon_{zz} E_z = i\lambda\partial_\xi E_x \tag{14}$$

$$i\,\partial_\tau E_x + \varepsilon E_x = i\lambda\partial_\xi E_z \tag{15}$$

where, the scaled variables $\tau = \omega t/2$, and $\xi = k_o x$ have been introduced. Furthermore, the simplifying notation $\partial/\partial\tau = \partial_\tau$, $\partial/\partial\xi = \partial_\xi$, $\lambda = k/k_o$, and $\varepsilon = \varepsilon_{xx} - \lambda^2$, is used.

To gain physical insight into the background of Eqs (14) and (15) it is useful to consider first the steady-state situation where $\partial_\tau \to 0$. In this special case Eq. (15) yields

$$E_x = \frac{i\lambda}{\varepsilon}\,\partial_\xi E_z \tag{16}$$

which can be inserted into Eq. (14) to obtain

$$\partial_\xi^2 E_z + \lambda^2 \frac{\varepsilon}{\varepsilon_{xx}}\,\partial_\xi\left(\frac{1}{\varepsilon}\right)\partial_\xi E_z + \frac{\varepsilon}{\varepsilon_{xx}}\,\varepsilon_{zz}\,E_z = 0 \tag{17}$$

Eq. (17) has the general form of a damped harmonic oscillator equation with variable coefficients. The contribution from the term proportional to $\partial_\xi E_z$ gives rise to a damping factor which is important only for extremely sharp gradients in the dielectrics. The coefficients multiplying the term proportional to E_z are of crucial importance to the behavior of the system because their combined sign determines whether or not the radiation can penetrate into the plasma. In those regions of extremely low density where $\omega_{pe}(x) < \omega$, it follows that $\varepsilon_{zz} < 0$. However, as one moves across the $\omega_{pe}(x) = \omega$ point, $\varepsilon_{zz} = 0$; finally, as one proceeds to the interior of the plasma where $\omega_{pe}(x) > \omega$, $\varepsilon_{zz} > 0$. Accordingly, the determining factor for the radiation to propagate beyond the $\omega = \omega_{pe}(x)$ point is that $\varepsilon/\varepsilon_{xx} < 0$. Since in this region $\varepsilon_{xx} \simeq 1$ this implies that $\varepsilon < 0$, or

$$\lambda^2 = \left(\frac{k}{k_o}\right)^2 > 1 \tag{18}$$

If this condition is satisfied then the external radiation mode-converts into an internal plasma oscillation which proceeds to propagate to the interior. However, the mode-converted oscillation can still be reflected at the point where $\varepsilon = 0$. Hence, if the mode-converted wave is ever to reach the lower-hybrid resonance this implies that

$$\lambda^2 = \left(\frac{k}{k_o}\right)^2 > 1 + \left(\frac{\omega_{pe}}{\Omega_e}\right)^2 \tag{19}$$

for all the density values up to the resonance layer. Eq. (19) is what one refers to as the accessibility criterion, which for the typical

parameters of relevance to thermonuclear fusion implies that $(k/k_o)^2 \gtrsim 2$, thus stressing the importance of using a carefully designed wave-launching structure.

For completeness, the solution of Eq. (17) illustrating the steady-state mode-conversion pattern for the simple case of a linear density gradient is given in Appendix A.

Having obtained an understanding of the steady-state response of the system one can return to the full space-time description provided by Eqs. (14) and (15). For the case $\lambda = 0$, it is clear that these equations decouple into two independent processes. Eq. (15) describes the behavior of local (i.e., non-propagating) electric field oscillations in the direction perpendicular to $\underset{\sim}{B}_o$. These local oscillations are not short circuited in either $\omega < \omega_{pe}(x)$ or $\omega > \omega_{pe}(x)$. Eq. (14) describes the propagation of electric field oscillations parallel to $\underset{\sim}{B}_o$. These oscillations propagate up to the $\omega = \omega_{pe}(x)$ point and are reflected back to the outside of the plasma. However, for $\lambda > 1$ these two independent oscillations couple to give rise to a net propagation of energy beyond the $\omega = \omega_{pe}(x)$ point. The crucial aspect of the propagation consists of the excitation of a localized oscillation in E_x by the gradient of E_z. Once this local oscillator is excited at a particular point in space, it permits the propagation of subsequent energy pulses. The resulting physical picture is that of a bootstrap mechanism whereby the Poynting vector of the incident radiation, which is initially aligned with $\underset{\sim}{B}_o$, is progressively rotated through a finite angle in the direction perpendicular to $\underset{\sim}{B}_o$.

The relation between the time evolution of the RF energy content of the system and the Poynting vector can be found from Eqs. (14) and (15). Multiplying Eq. (14) by E_z^*, Eq. (15) and E_x^* and subtracting the complex conjugate of the resulting expression yields

$$i\,\partial_\tau[|E_x|^2 + |E_z|^2] + (E_z^*\partial_\xi^2 E_z - \text{c.c.})$$

$$+ 2i\,[\mathrm{Im}(\varepsilon_{zz})\,|E_z|^2 + \mathrm{Im}(\varepsilon_{xx})\,|E_x|^2] \qquad (20)$$

$$= 2i\lambda\,\mathrm{Re}[\partial_x(E_z^* E_x)]$$

Next, integrate both sides of Eq.(20) from an initial point ξ_o, located outside the plasma, up to a point ξ_f, deep inside the plasma. At ξ_o, E_z is assumed to be fixed by the wave-launching structure, while at ξ_f, $E_x = E_z = 0$ because the RF energy has not had enough time to propagate to this point. Performing the integration yields an expression of the form

$$i\,\frac{2k_o}{\omega}\,\frac{\partial}{\partial t}\,U + i\,2k_o\,\frac{\langle\gamma\rangle}{\omega}\,U = I_1 + I_2 \qquad (21)$$

where,

$$U = \int_{x_o}^{x_f} dx\,[|E_x|^2 + |E_z|^2] \qquad (22)$$

represents the instantaneous electric field energy per unit area stored in the region bounded by the points x_o and x_f (corresponding to ξ_o and ξ_f). In Eq. (21)

$$\frac{\langle\gamma\rangle}{\omega} = \frac{\displaystyle\int_{x_o}^{x_f} dx\,[\mathrm{Im}(\varepsilon_{xx})\,|E_x|^2 + \mathrm{Im}(\varepsilon_{zz})\,|E_z|^2]}{U} \qquad (23)$$

represents, physically, the average rate of energy absorption or heating which takes place between x_o and x_f. The remaining terms in Eq.(21) are

$$I_1 = -\frac{1}{k_o}\int_{x_o}^{x_f} dx\ (E_z^*\ \partial_x^2\ E_z - C.C.) \tag{24}$$

which upon integration by parts yields

$$I_1 = \frac{1}{k_o}\ (E_z^*\ \partial_x\ E_z - C.C.)$$

$$I_1 = \frac{2i}{k_o}\ \mathrm{Im}(E_z^*\ \partial_x\ E_z)_{x_o} \tag{25}$$

similarly,

$$I_2 = i\lambda \int_{x_o}^{x_f} dx\ (E_z^*\ \partial_x\ E_x + E_x^*\ \partial_x\ E_z + C.C.) \tag{26}$$

hence,

$$I_2 = -2i\lambda\ \mathrm{Re}(E_x E_z^*)_{x_o} \quad . \tag{27}$$

Combining Eqs. (21) through (26) one obtains

$$\frac{\partial}{\partial t} U + \langle\gamma\rangle U = -\frac{\omega}{k_o^2}\ \mathrm{Im}(E_z^*\ \partial_x\ E_z)_{x_o} - \frac{\omega}{k_o}\ \lambda\ \mathrm{Re}(E_x\ E_z^*)_{x_o} \quad . \tag{28}$$

The terms on the left-hand side of Eq. (28) can be readily interpreted; they simply represent the rate of change of the total electric field energy per unit area contained in the system. The meaning of the right-hand side of Eq.(28) is made clear by evaluating the Poynting vector $\underset{\sim}{S}$ at x_o

$$4\pi\ \underset{\sim}{S} = c\ \mathrm{Re}\ (\underset{\sim}{E} \times \underset{\sim}{B}^*) \tag{29}$$

but,

$$\underset{\sim}{B} = \nabla \times \underset{\sim}{E}/(ik_o) \tag{30}$$

hence

$$\underset{\sim}{B} = \hat{y}(ikE_x - \partial_x E_z)/(ik_o) \tag{31}$$

where $\hat{y}$ is the unit vector in the y direction. Accordingly,

$$4\pi\underset{\sim}{S} = \frac{c}{k_o} \mathrm{Re}[(i\partial_x E_z^* - kE_x^*)(E_z\hat{x} - E_x\hat{z})] \tag{32}$$

thus,

$$4\pi\underset{\sim}{S}\cdot\hat{x} = \frac{c}{k_o} [\mathrm{Re}(iE_z\partial_x E_z^*) - k\ \mathrm{Re}(E_z E_x^*)] \tag{33}$$

but,

$$\mathrm{Re}(iE_z\partial_x E_z^*) = -\ \mathrm{Im}(E_z\partial_x E_z^*) \tag{34}$$

hence,

$$4\pi S_x = -\frac{c}{k_o} \mathrm{Im}(E_z\partial_x E_z^*) - c\lambda\ \mathrm{Re}(E_z E_x^*) \tag{35}$$

which exactly reproduces the right-hand side of Eq. (28) when evaluated at $x = x_o$. The interpretation of Eq. (28) is now complete, it reads simply

$$\frac{d}{dt} U = 4\pi(S_x)_{x_o} \tag{36}$$

thus stating that the increase in the electric field energy content of the plasma arises due to the development of a non-zero S_x just outside the plasma edge.

To understand the nature of the external radiation in this problem it is useful to consider the system in the absence of plasma. In this case, $\varepsilon_{zz} = \varepsilon_{xx} = 1$, and $\varepsilon = 1 - \lambda^2 < 0$. Hence, Eq. (17) takes the form

$$\partial_\xi^2 E_z - (\lambda^2 - 1)E_z = 0 \tag{37}$$

whose solution is

$$E_z = E_o \exp(-[\lambda^2 - 1]^{1/2} k_o x) \tag{38}$$

thus indicating that the external radiation is evanescent in the direction in

which the plasma density increases (i.e., when the plasma is present). In Eq. (38) E_o is a real coefficient which represents the peak field produced by the wave-launching structure in vacuum.

The energy flow associated with the external radiation is found by evaluating the Poynting vector from Eq. (32), in which

$$E_x = \frac{i\lambda}{1-\lambda^2}\,\partial_\xi E_z \tag{39}$$

hence,

$$4\pi \underset{\sim}{S} = \frac{c}{k_o}\,\mathrm{Re}\left[\frac{i\,\partial_x E_z}{1-\lambda^2}\,(\hat{x}E_z - \hat{z}E_x)\right] \tag{40}$$

and since E_x is purely imaginary and given by

$$E_x = \frac{i\lambda}{[\lambda^2-1]^{1/2}}\,E_x \tag{41}$$

it follows that

$$S_x = 0$$

$$4\pi S_z = \frac{c\lambda}{\lambda^2-1}\,E_o^{\,2}\,\exp[-2(\lambda^2-1)^{1/2}\,k_o x] \quad . \tag{42}$$

Equation (42) illustrates that the external radiation transports energy only in the direction of $\underset{\sim}{B}_o$ and that the magnitude of this flow decreases exponentially in the direction of increasing plasma density. Accordingly, the picture of the system at a time shortly before mode-conversion occurs is as illustrated qualitatively in Fig. 2.

The nature of the oscillations excited in the mode-conversion process can be better understood by examining the dependence of the generated S_x on the phase of the mode-converted waves. This relationship is simpler to examine for the steady-state case in which the electric field components have the form

$$E_z(x) = \alpha(x)\, \exp[ia(x)]$$

$$E_x(x) = \beta(x)\, \exp[ib(x)] \qquad (43)$$

where (α, β) and (a, b) are real functions describing the amplitude and phase of the (E_z, E_x) components. Using Eq. (31) leads to

$$4\pi S_x = \frac{c}{k_o} \mathrm{Re}[i(\partial_x \alpha - i\alpha \partial_x a)\, e^{-ia} - k\beta\, e^{-ib}]$$

$$4\pi S_x = \frac{c}{k_o} [\alpha^2 \partial_x a - k\alpha\beta \cos(a-b)] \quad . \qquad (44)$$

Again, in the region of interest $\varepsilon_{xx} \simeq 1$, $\varepsilon_{xx} \simeq 1-\lambda^2$ hence

$$E_x = \frac{i\lambda}{1-\lambda^2} \frac{1}{k_o} \frac{\partial}{\partial x} E_z \qquad (45)$$

implying that

$$\beta = \left(\frac{\lambda}{\lambda^2-1}\right) \left(\frac{1}{k_o}\right) [(\alpha \partial_x a)^2 + (\partial_x \alpha)^2]^{1/2} \qquad (46)$$

and $b-a = \phi$, with

$$\phi = \tan^{-1} \left(\frac{-\partial_x \alpha}{\alpha \partial_x a}\right) \qquad (47)$$

thus Eq. (44) takes the form

$$4\pi S_x = \frac{c}{k_o} \{\alpha^2 \partial_x a - \frac{\lambda^2}{\lambda^2-1} \cos\phi\, [(\alpha \partial_x a)^2 + (\partial_x \alpha)^2]^{1/2}\} \qquad (48)$$

using Eq. (47) leads to

$$4\pi S_x = \frac{c}{k_o} \alpha^2 \partial_x a \left[1 - \frac{\lambda^2}{\lambda^2-1}\right]$$

or (49)

$$4\pi S_x = -\frac{c}{k_o} \alpha^2 \frac{\partial_x a}{\lambda^2-1}$$

Since $\lambda^2 > 1$ to satisfy the accessibility criterion, Eq. (49) in conjunction with Eq. (36) implies that in order to couple RF energy to the interior of the plasma the oscillations excited by the mode-conversion process must be strictly of the backward type, i.e.,

$$\partial_x a < 0 \qquad (50)$$

In principle, Eqs. (14) and (15) can be transformed into an integral representation by using a double Laplace transform in τ and ξ. However, the resulting expressions are not of much use when actually trying to display the space-time evolution of the electric field. In particular, this task is rather arduous for complicated density profiles and is only limited to linear problems. A more direct approach is to solve Eqs. (14) and (15) by using difference schemes in a digital computer. In this manner one can handle arbitrary density profiles, complicated boundary conditions, and in addition it permits the investigation of important nonlinear effects. The implementation of such a numerical study for Eqs. (14) and (15) is discussed briefly in Sec. III. For completeness, the integral representation of Eqs. (14) and (15) is given in appendix B for the simple case of a constant density profile.

The space-time formulation provided by Eqs. (14) and (15) permit the description of numerous linear and nonlinear processes which arise due to the explicit dependences of ε_{xx} and ε_{zz} on the plasma parameters. Some of these parameters may contain interesting zero-order fluctuations of their own, or can be altered in a nonlinear manner when the applied radiation is rather intense. An interesting problem associated with natural fluctuations is the purely linear backscattering of the evanescent radiation by surface ripples. This is a process which may inhibit the rotation of $\underset{\sim}{S}$ by a significant angle, however, its investigation is outside the scope of the present study.

Out of the many nonlinear processes that may arise at the edge of the plasma when large power levels are applied in a heating experiment, in the present study we have chosen to isolate the specific effects associated with the modification of the density profile by the ponderomotive force. This is an effect whose consequences may be of importance because it alters directly the process of mode-conversion by shifting the point where $\omega = \omega_{pe}(x)$ and simultaneously changes the gradient scale length. As it has been seen earlier

in this section, the mode-conversion process is responsible for the generation of a non-zero S_x, thus the profile modification can play an inhibiting role in the coupling of RF energy at large power levels. It is also of general interest to compare the effects of the nonlinear density changes in the present magnetized plasma problem with those previously observed experimentally[12] and theoretically[13] in the interaction of intense evanescent radiation in an unmagnetized plasma.

For the sake of simplicity, in the present study we introduce the nonlinear profile modification explicitly through the expression for the plasma density, i.e., by using

$$n(x, |\underset{\sim}{E}|^2) = n_o(x) \exp\left[-\frac{|\underset{\sim}{E}|^2}{4\pi n_o(x) T}\right] \tag{51}$$

in which n_o represents the spatially dependent zero-order density (i.e., unmodified), T is the plasma temperature, and $|\underset{\sim}{E}|^2$ is to be determined self-consistently from Eqs. (14) and (15). The nonlinear density shown in Eq. (51) appears in Eqs. (14) and (15) through the expression $\omega_{pe}^2 = 4\pi e^2 n(x, |\underset{\sim}{E}|^2)/m$ contained in the dielectrics.

Clearly, Eq. (51) is an oversimplification of the actual behavior of the plasma density which is subjected to the intense power levels expected in a fusion-grade experiment. Immediately, in a problem of this nature one can think of including a variety of effects, such as the generation of ion acoustic waves, shocks, plasma heating, etc. However, before proceeding to include such complications one must assess what results arise from the simple model provided by Eq. (51). Such is the philosophy behind the nonlinear studies presented in Sec. IV.

III. NUMERICAL PROCEDURE

In implementing the numerical study of the mode-conversion process one proceeds first to discretize the time variable in finite increments $\Delta\tau$, and to time-average both Eqs. (14) and (15) to obtain

$$\frac{i}{\Delta\tau}(F-\not{F}) + \frac{1}{2}\partial_\xi{}^2(F+\not{F}) + \frac{\varepsilon_{zz}}{2}(F+\not{F}) = \frac{i\lambda}{2}\partial_\xi(G+\not{G}) \tag{52}$$

$$\frac{i}{\Delta\tau}(G-\not{G}) + \frac{\varepsilon}{2}(G+\not{G}) = \frac{i\lambda}{2}\partial_\xi(F+\not{F}) \tag{53}$$

where $F = E_z(\xi, \tau)$, $G = E_x(\xi, \tau)$ represent the present values of the electric field components, and $\not{F}$, $\not{G}$ refer to their value at the previous time step, e.g., $\not{A} = A(\xi, \tau-\Delta\tau)$. Eqs. (52) and (53) provide a coupling between F and G which must be solved implicitly at every time step.

Eliminating G from Eq. (53) gives

$$G = \frac{\not{G}[(i/\Delta\tau) - (\varepsilon/2)] + i\frac{\lambda}{2}\partial_\xi(F+\not{F})}{i/\Delta\tau + \varepsilon/2} \tag{54}$$

which can be inserted in Eq. (52) to yield

$$\partial_\xi{}^2 F + \frac{[(i/\Delta\tau) + (\varepsilon/2)]}{[(i/\Delta\tau) + (1/2)]}\left[\frac{2i}{\Delta\tau} + \varepsilon_{zz}\right]F = -\partial_\xi{}^2\not{F} - \frac{2\lambda}{\Delta\tau}\frac{\partial_\xi\not{G}}{\frac{i}{\Delta\tau}+\frac{1}{2}} + \frac{[(i/\Delta\tau) + (\varepsilon/2)]}{[(i/\Delta\tau) + (1/2)]}\left[\frac{2i}{\Delta\tau} - \varepsilon\right]\not{F} \tag{55}$$

in which one makes explicit use of the simplifying properties of the edge region, namely $\varepsilon_{xx} \simeq 1$. Eq. (55) provides a second order ordinary differential equation for the present value of E_z. This equation can be solved implicitly if one knows the previous value of E_z, the spatial dependence of the dielectric ε_{zz}, and the appropriate boundary conditions.

To solve Eq. (55) one goes through an averaging and discretization in ξ, similar to that used in generating Eqs. (52) and (53). The resulting second difference equation in ξ is solved implicitly by using the well-known[14] tri-diagonal algorithm. After having calculated F by this method one returns to Eq. (54) to update G, thus completing one full time step in the problem.

The boundary conditions used in solving the present problem are the following: 1) E_z is held fixed at the value E_o at a position well outside the plasma, and 2) $E_z = 0$ at the boundary located deep inside the plasma. The exact location of the point outside the plasma has been varied for a given density profile to verify that the results are independent of its particular numerical value. Similar sensitivity studies have been made concerning the incremental space-time steps $\Delta\xi$ and $\Delta\tau$. To insure that no reflection problems develop with the $E_z = 0$ boundary at late times in the evolution, a strong edge absorption is included through ϵ_{zz}; this boundary absorption does not give rise to observable effects in the region of interest here.

The choice of boundary condition outside the plasma allows maximum freedom to the mode-conversion process, since the value of $\partial_\xi E_z$ is left unspecified, as should be the case. This derivative, as well as the value of E_x at the outside boundary is allowed to evolve self-consistently in time, so their combination gives rise to the gradual development of a finite S_x.

The initialization of the system is accomplished by assigning the steady-state, pure vacuum solution to the quantities E_z and E_x, i.e., they are given the values predicted by Eqs. (38) and (39). This procedure can be interpreted physically as a statement that prior to the development of the mode-conversion process the plasma is virtually insensitive to the RF fields. However, a few cycles after turning-on the oscillator the plasma begins to respond, and it is this time that we arbitrarily denote as $t = 0$. Of course, one can also consider the slow turn-on problem in which one legislates E_o to be a slowly increasing function of time, however no additional physical insight is gained by this procedure which introduces further arbitrary choices of parameters.

Various shapes of the zero-order density profile $n_o(x)$ have been investigated in which in general the density is taken to increase monotonically

as a function of x. Although for each individual profile the spatial scale of the fields developed is observed to vary in the expected manner, the general features presented in Sec. IV are insensitive to the specific choice of profile.

Finally, the nonlinear density profile given by Eq. (51) is introduced into the numerical scheme, at a given time step, by averaging the quantity $|\underset{\sim}{E}|^2$ over the two previous time steps. In this manner a certain amount of numerical inertia is retained in the method.

We proceed next to discuss the results obtained by implementing this numerical scheme with the help of the mathematical on-line system at the University of California, Los Angeles.

IV. RESULTS

A. Linear Behavior

In the investigation of Eqs. (14) and (15) a particular zero-order density profile must be chosen. In general, we characterize the profiles used by means of a single scale-length L, i.e., $n_o = n_o(x/L)$. Thus, it proves convenient for display as well as for physical reasons to scale the spatial variable in terms of this natural length of the problem. This choice implies that in the linear regime the system depends explicitly on two lumped parameters, namely $k_o L$ and $\lambda = k/k_o$. The results to be presented correspond to the particular choice $\lambda^2 = 2$, which is representative of the expected experimental values. In addition, the parameter regime of interest to the physics of the plasma edge corresponds to $k_o L \sim 1$.

To give a feeling for the numbers that these choices may imply for actual applications, it should be noted that for incident radiation having a frequency $\upsilon = \omega/2\pi \sim 3$ GHZ, which may be considered typical of a fusion-grade experiment, the length scale corresponds to $L \sim 1$ cm. However, for the purposes of the present study no specific values of ω and L need to be assigned.

A characteristic density profile used in the present studies is indicated by the solid curve shown in Fig. 3. It corresponds to the choice

$$\frac{n_o(x)}{n_p} = [1 + \tanh (\frac{x}{L} - 4)] \; (x/2L) \tag{56}$$

where, n_p represents the density for which $\omega_{pe}(x) = \omega$, and whose numerical value does not need to be specified. The dashed curve in Fig. 3 is the dielectric ε_{zz}; its zero-crossing separates the evanescent and propagating regions. The dotted curve in Fig. 3 is the quantity $|\underset{\sim}{E}|^2$ prior to the development of the mode-conversion process; its strong evanescence into the plasma is apparent.

It should be emphasized that the results to be presented in the remainder of this subsection are strictly linear, i.e., the nonlinear density profile given by Eq. (51) is replaced by n_o, the zero-order unperturbed profile.

The space-time evolution of the process of linear mode-conversion is illustrated in Fig. 4, in which we plot the spatial dependence of the real and imaginary parts of E_z for various different times. These results are obtained for the profile shown in Fig. 3, and the values $k_o L = 1$, $(k/k_o)^2 = 2$. It should be noted that there is a change in the spatial grid between the displays of Figs. 3 and 4. In Fig. 4(a) $\upsilon t = 1.0$, hence the early pattern observed is essentially the evanescent vacuum solution except for the appearance of the small imaginary part near the edge. By $\upsilon t = 5.0$ it is seen in Fig. 4(b) that the small imaginary part of Fig. 4(a) has grown in amplitude and in doing so it becomes spatially out of phase with the real part. The combined real and imaginary parts have developed by this time almost a full wavelength which extends into the plasma beyond the point where $\varepsilon_{zz} = 0$. In Fig. 4(c) one clearly observes the development in the interior of the plasma of a wave which is continuously linked to the evanescent external radiation in the region $x/L \sim 3$ (i.e., near $\varepsilon_{zz} = 0$). Fig. 4(d) at $\upsilon t = 20.0$ indicates the existence of a well-defined propagating wavepacket having a significant amplitude and whose role is to transport the RF energy to the interior of the plasma.

The transport of RF energy associated with the sequence of events illustrated in Fig. 4 can be seen in Fig. 5. In this figure we reproduce the information of Fig. 3, but include in it the spatial dependence of the mode-converted quantity $|E_z|^2$ for $\upsilon t = 20.0$ (represented by the dotted curve). For reference it should be mentioned that in the absence of mode-conversion the quantity $|E_z|^2$ would be evanescent beyond the $\varepsilon_{zz} = 0$ point.

Although the sequence of events depicted in Fig. 4 clearly indicate that RF energy is being carried away from the edge toward the interior of the plasma, it is not clear from this presentation if the excited mode corresponds to a

forward or to a backward wave. To check on this feature one needs to plot a phasor diagram akin to that commonly used in sampling-time interferometric measurements of plasma waves. Such a plot is given in Fig. 6 for the E_z component at the fixed time $\upsilon t = 5.0$, and obtained for a profile which differs slightly from that shown in Fig. 3. In Fig. 6 the direction of the arrows indicate the direction of increasing density, or equivalently, to penetrating deeper into the plasma. The fact that in Fig. 6 the phasor rotates in the clockwise direction (i.e., in the direction of decreasing phase angle) identifies the type of modes shown in Fig. 4 as being backward waves, as is expected from the analysis leading to Eq. (50). The corresponding behavior for the E_x component is illustrated in Fig. 7.

It has been demonstrated in Figs. 4 through 7 that the process of linear mode-conversion indeed takes place as expected and that it generates a backward wavepacket that proceeds to fill the interior of the plasma with RF energy. Having observed the evolution of this process it is of interest to inquire how the steady-state is attained for a given spatial point in the region where $\varepsilon_{zz} > 0$. The answer to this question is provided by the sequence of curves shown in Fig. 8. In this figure we plot the total electric field energy density $|\underset{\sim}{E}|^2$ as a function of spatial location with time as the parameter being varied over the interval $0.5 \leq \nu t \leq 10.0$. Again, this result is obtained for a profile slightly different from that of Fig. 3, and with $k_o L = 1$, $(k/k_o)^2 = 2$. The salient feature uncovered by Fig. 8 is that the RF energy propagates away from the $\varepsilon_{zz} = 0$ region via a leading-edge pulse which grows in amplitude spatially as it penetrates deeper into the plasma. At a fixed spatial location, however, nothing occurs in time until the foot of the pulse arrives. After its arrival at a given point the local energy density grows in time until the peak of the leading-edge pulse passes by. Shortly after the passage of the propagating

pulse, the amplitude of the local energy density stops growing and attains its steady-state value. The attainment of the steady-state is reflected in Fig. 8 by the accurate overlapping of all curves in the trailing edge of the propagating pulse.

B. Nonlinear Behavior

We proceed next to describe the results obtained when the nonlinear density modification given by Eq. (51) is included in the space-time evolution of the mode-conversion process. A characteristic profile distortion produced at the edge of the plasma is shown in Fig. 9. In this figure the dashed curve corresponds to the zero-order unperturbed density, while the continuous curve is the nonlinearly modified profile at $\upsilon t = 10.0$, for $k_o L = 1$, and $(k/k_o)^2 = 2$.

Three qualitatively different types of distortions can be identified in Fig. 9, namely: 1) the recession of the point $\omega_{pe}(x) = \omega$ away from the wave-launching structure; 2) the local steepening of the profile at the newly created $\omega_{pe}(x) = \omega$ point; and 3) the generation of density pockets or striations beyond this point. All of these distortions work in the direction of decreasing the effectiveness of the mode conversion process, hence the nonlinearity in this problem is self-limiting in the sense that the distortion leads to a reduction of $|\underset{\sim}{E}|^2$ inside the plasma instead of enhancing it. This behavior is quite the opposite of that observed in the mode-conversion problem in an unmagnetized plasma. As is well known,[12,13] in the unmagnetized case the generation of density cavities localizes the electric field and leads to the formation of high intensity spikes.

The quenching effect produced on the mode-converted wave by the modification of the profile is illustrated in Fig. 10 for a study made with a zero-order density of the form $n_o/n_p = x/L$, and with $k_o L = 1$, $(k/k_o)^2 = 2$. Fig. 10 is a phasor plot of E_z (of the type discussed earlier in connection with Fig. 6) in which we present, on the same scale, the patterns obtained for a strictly

linear case, Fig. 10(a), and for a strongly nonlinear run, Fig. 10(b). The nonlinear result shown is obtained with an initial external excitation level (i.e., E_o in Eq. (38) that produces an initial value of $|\tilde{E}|^2/(4\pi n_o T) = 7$ at the point where $\omega_{pe}(x) = \omega$.

It is clearly seen in Fig. 10 that the nonlinearity reduces the amplitude of the mode converted wave, thus producing a significant quenching in the amount of RF energy that penetrates to the interior of the plasma.

The salient features observed in Fig. 10(b) are: 1) the increased evanescence (straight-line pattern) due to the recession of the $\omega = \omega_{pe}(x)$ point to the interior; 2) the appearance of an abrupt phase change associated with the increased steepness of the profile (manifested through the rapid transition from straight-line to a curve); and 3) an overall retardation in the evolution of the mode-converted wave relative to the linear case. A similar quenching occurs also in the E_x component, as is illustrated in Fig. 11 for a case $k_o L = 2$, $(k/k_o)^2 = 2$, and in which the chosen E_o yields $|\tilde{E}|^2/(4\pi n_o T) = 0.5$ at the ω_{pe} point initially.

A convenient method of assessing the overall effect of the nonlinearity consists of evaluating the instantaneous RF energy content of the plasma slab considered, i.e., by calculating the normalized quantity

$$u(t) \equiv \frac{U(t)}{E_o^2} = \frac{\int_{x_1}^{x_2} dx |\tilde{E}|^2}{E_o^2} \qquad (57)$$

where, x_1 and x_2 refer to the boundaries of the slab. In Eq. (57) the division by E_o^2 removes the trivial dependence on the external driver amplitude, therefore any changes obtained in u(t) by varying E_o are due to explicit nonlinear changes in the profile. Such a dependence is illustrated in Fig. 12 for an initial profile $n_o/n_p = x/L$, $k_o L = 1$, and $(k/k_o)^2 = 2$. The top curve corresponds to a strictly linear case (i.e., the nonlinearity is shut-off), while the other curves

correspond to initial values of $|E|^2/(4\pi n_o T)$ at the ω_{pe} point of 0.4, 1.6, and 3.6 respectively.

It is evident from Fig. 12 that as one increases the external power in the wave-launching structure, the relative amount of RF energy which actually penetrates into the plasma decreases steadily. This result can be interpreted in the practical sense as saying that the RF-plasma coupling at the surface is a decreasing function of the applied power. Physically, of course, this means that the nonlinear quenching of the mode-conversion process decreases the angle through which the Poynting vector can be rotated.

From the results of Fig. 12 one can extract the rate at which the plasma slab is filled with RF energy, i.e., by calculating the quantity

$$\frac{\overline{V}}{c} \equiv \frac{d}{dt}\ \frac{u(t)}{c} \tag{58}$$

in which u(t) is defined by Eq. (57) and the speed of light, c, proves to be a convenient scaling factor since the quantity $\overline{V}$ denotes an effective speed of energy propagation into the plasma. Clearly, the quantity $\overline{V}/c$ can also be interpreted as the scaled Poynting vector perpendicular to $\underset{\sim}{B}_o$.

The amplitude dependence of $\overline{V}/c$ is illustrated in Fig. 13 for the results previously shown in Fig. 12. The accentuated squares in Fig. 13 denote the numerical results, and the continuous curve is an excellent eyeball-fit given by the expression

$$\frac{\overline{V}}{c} = (0.11)\ \exp\ [-(1.3)\ \sqrt{p}] \tag{59}$$

where $p = |\underset{\sim}{E}|^2/(4\pi n_o T)$ at the $\omega_{pe}(x) = \omega$ point prior to mode-conversion.

It is of interest to inquire what effect the nonlinearity has on the behavior of the propagating leading-edge pulse, observed in the linear regime and whose evolution is shown in Fig. 8. A characteristic nonlinear response is exhibited in Fig. 14, in which we present the spatial dependence of $|\underset{\sim}{E}|^2$ and n for different times in the interval $5.0 \leq \nu t \leq 10.0$, for the case $k_o L = 1$,

$(k/k_o)^2 = 2$, and for the initial profile indicated by the dashed curve.

It is seen in Fig. 14 that the leading-edge pulse, characteristic of the linear regime,breaks up into an isolated peak which proceeds to propagate into the plasma. The isolated peak observed in Fig. 14(c) is reminescent of a Langmuir-wave soliton and its associated density cavity. However, the reason for the localization of the pulse in Fig. 14(c) is entirely different from the Langmuir-wave case. In the Langmuir-wave soliton the localization is associated with the trapping of the radiation in a density cavity, while in here no trapping phenomena occurs. In here, the isolated pulse arises because its leading edge modifies the profile thus reducing the efficiency of mode-conversion for pulses that trail in time. In other words, the leading edge samples the higher efficiency zero-order profile, while the trailing edge samples the modified profile which has lower efficiency for mode conversion.

The nonlinearly generated RF pulses can become quite dramatic in their appearance for shallow density profiles, i.e., when $\omega_{pe}(x)$ does not become too large compared to ω. An example of the sharp pulses that can appear in these cases is shown in Fig. 15, which has been obtained with $n_o/n_p = 2\ [1+\tanh(\frac{x}{L}-4)]$ for $k_oL = 1, (k/k_o)^2 = 2$, and $|\underset{\sim}{E}|^2/(4\pi n_oT) = 6.0$ at the $\omega = \omega_{pe}$ point, initially. The time of observation in Fig. 15 corresponds to $\upsilon t = 13.0$.

It is clear from the nonlinear physics that underlies the generation of the pulses exemplified in Figs. 14 and 15, that multiple peaks or pulse-trains should appear in the long time evolution of the system. The reason is simply that the nonlinearity is self-limiting, hence after the passage of a large amplitude peak the system returns to its linear behavior which proceeds to generate another linear leading-edge pulse, and thus the cycle repeats. The generation of multiple-peak pulses can also be interpreted by saying that the x component of the Poynting vector, S_x, is constantly oscillating between its

linear and nonlinear values, thus leading to an intermittent flow of RF energy into the plasma.

The existence of these multiple-peak pulses or pulse trains is indicated in Fig. 16, in which we display the spatial dependence of $|E_x|^2$ for various times in the interval $10.0 \leq \upsilon t \leq 14.0$ and obtained for a case $n_o/n_p = x/L$, $k_o L = 1$, $(k/k_o)^2 = 2$, and $|\underset{\sim}{E}|^2/(4\pi n_o T) = 3.0$ at $\omega = \omega_{pe}(x)$, initially. In Fig. 16(a) one observes a dominant single peak located near the left boundary and followed by two small pulses. Fig. 16(b) shows that the pattern of Fig. 16(a) propagates into the plasma, with the trailing pulses becoming more visible. Finally, in Fig. 16(c) one observes a fully developed multiple-peak pulse train that transports the RF energy to the interior of the plasma.

V. SUMMARY

In the present investigation the use of a modulational representation for the electric field has permitted the full description, in the linear as well as in the nonlinear regime, of the process of mode-conversion encountered at the edge of the plasma in the lower-hybrid heating scheme.

It has been found that the salient feature of the mode-conversion process consists of the gradual excitation of a backward wave which causes a rotation of the Poynting vector of the external evanescent radiation in the direction of the density gradient, thus allowing the RF energy to penetrate into the plasma.

The transient transport of RF energy away from the plasma edge toward the interior has been found to be accomplished by the propagation of a leading-edge pulse whose arrival at a given spatial location denotes the onset of the steady-state.

It has been found that the nonlinear profile modification produced by a simplistic mode of the ponderomotive force can cause a significant quenching of the mode-conversion process, thus reducing the amount of RF energy that can be coupled to the interior of the plasma at large power levels. These results thus warrant future studies in which more complicated and realistic models of the profile modification are used.

In the strongly nonlinear regime the present study has uncovered new and interesting multiple-peak pulse trains that can be quite striking in shallow density profiles. The consequence of the existence of these nonlinear pulses is that the flow of RF energy to the interior of the plasma is intermittent at large power levels.

ACKNOWLEDGEMENT

The present work has been supported by the U. S. Energy Research and Development Agency through contract E(11-1)Gen. 10 PA26, and by the Office of Naval Research through contract ONR N00014-75-C-0476 P00002.

APPENDIX A

Consider the special case in which $\omega_{pe}^2(x)/\omega^2 = 1 + x/L$, and where $x > 0$ denotes the interior of the plasma. Accordingly,

$$\frac{d}{d\xi}\left(\frac{1}{\varepsilon}\right) = -\frac{1}{\varepsilon}\left[\left(\frac{\omega}{\Omega_e}\right)^2 - \frac{m}{M}\right]\frac{1}{k_o L} \tag{A-1}$$

and Eq. (17) becomes

$$\frac{d^2}{d\xi^2}E_z - \frac{\lambda^2}{\varepsilon\varepsilon_{xx}}\left[\left(\frac{\omega}{\Omega_e}\right)^2 - \frac{m}{M}\right]\frac{1}{k_o L}\frac{d}{d\xi}E_z + \frac{\varepsilon}{\varepsilon_{xx}}\varepsilon_{zz}E_z = 0 \quad . \tag{A-2}$$

Defining,

$$E_z(\xi) = f(\xi)\exp\left[\int_{-k_o L}^{\xi} d\xi'\, g(\xi')\right] \tag{A-3}$$

with

$$g = \frac{\lambda^2}{2\varepsilon\varepsilon_{xx}}\left[\left(\frac{\omega}{\Omega_e}\right)^2 - \frac{m}{M}\right]\frac{1}{k_o L} \tag{A-4}$$

yields,

$$\frac{d^2}{d\xi^2}f + \left[\frac{\varepsilon\varepsilon_{zz}}{\varepsilon_{xx}} - g^2\right]f = 0 \quad . \tag{A-5}$$

In the region of interest $\varepsilon_{xx} \simeq 1$ and $\varepsilon \simeq 1-\lambda^2$, thus

$$\frac{d^2}{d\xi^2}f + \left[\left(\frac{\lambda^2-1}{k_o L}\right)\xi - g^2\right]f = 0 \quad . \tag{A-6}$$

Defining $\xi = [k_o L/(\lambda^2-1)]^{1/3}\eta$ produces

$$\frac{d^2}{d\eta^2}f + (\eta-\eta_o)f = 0 \tag{A-7}$$

with $\eta_o = g^2[k_o L/(\lambda^2-1)]^{2/3}$. The general solution of (A-7) has the form

$$f = \gamma A_i(\eta-\eta_o) + \delta B_i(\eta-\eta_o) \tag{A-8}$$

where γ and δ are constants to be determined, and A_i, B_i refer to the Airy functions defined in Ref. (15). Requiring that as $\eta \to \infty$ (i.e., $x \to \infty$) the solution should describe the transport of energy into the plasma implies $\delta = i\gamma$.

Accordingly, the steady-state linear mode-conversion has the solution

$$E_z(x) = \gamma \left[A_i \left(\frac{kx}{L} - \eta_o \right) + iB_i \left(\frac{kx}{L} - \eta_o \right) \right] \exp\left\{ \lambda^2 \left[\left(\frac{\omega}{\Omega_e} \right)^2 - \frac{m}{M} \right] \left(1 + \frac{x}{L} \right) \right\} \qquad \text{(A-9)}$$

where $k = (\lambda^2-1)^{1/3} (k_o L)^{2/3}$, and the remaining constant γ is determined by the amplitude of the external radiation.

APPENDIX B

Defining $A = E_z$, $B = E_x$, Eqs. (14) and (15) become

$$i\,\partial_\tau A + \partial_\xi^2 A + \varepsilon_{zz} A = i\lambda\partial_\xi B$$

$$i\,\partial_\tau B + \varepsilon B = i\lambda\partial_\xi A \quad . \tag{B-1}$$

Introducing the Laplace transform operator in time

$$\mathcal{L}_s = \mathcal{L}(s;\tau)\ \{\ \} = \int_0^\infty d\tau\, e^{s\tau}\ \{\ \} \tag{B-2}$$

and $\mathcal{L}_s A = \tilde{A}$, $\mathcal{L}_s B = \tilde{B}$, yields

$$\partial_\xi^2 \tilde{A} + \left(\frac{\varepsilon+is}{\varepsilon_{xx}+is}\right)(\varepsilon_{zz}+is)\tilde{A} = i\left(\frac{\varepsilon+is}{\varepsilon_{xx}+is}\right)A(\xi,\tau=0) - \frac{i\lambda}{\varepsilon_{xx}+is}\,\partial_\xi B(\xi,\tau=0) \tag{B-3}$$

Further introduction of a Laplace transformation in space, in the manner shown in (B-2), i.e., $\mathcal{L}_k = \mathcal{L}(k;\xi)$ and $\mathcal{L}_k\mathcal{L}_s A = \bar{\tilde{A}}$ transforms (B-3) to the form

$$[k^2+K^2(s)]\bar{\tilde{A}} = \left(\frac{\partial}{\partial\xi}\tilde{A}\right)(\xi=0,s) + k\tilde{A}(\xi=0,s) + i\left(\frac{\varepsilon+is}{\varepsilon_{xx}+is}\right)\bar{A}(k,\tau=0) - \frac{i\lambda}{\varepsilon_{xx}+is}\,\overline{\partial_\xi B}(k,\tau=0) \tag{B-4}$$

where, $K^2(s) = (\varepsilon+is)(\varepsilon_{zz}+is)/(\varepsilon_{xx}+is)$ and it is explicitly assumed that the dielectrics are spatially independent. If a spatial dependence were allowed, then (B-4) would become an integral equation involving appropriate convolutions of the dielectrics and fields.

Using the pure vacuum radiation solutions to evaluate $A(\xi,\tau=0)$ and $B(\xi,\tau=0)$ through

$$A = a\,\exp[-(|\varepsilon/\varepsilon_{xx}|)^{1/2}\,\xi]$$

$$B = -\frac{i\lambda}{(|\varepsilon|\ |\varepsilon_{xx}|)^{1/2}}\,A \tag{B-5}$$

where a denotes the peak field amplitude produced by the wave-launching

structure, yields

$$A(x,t) = \int \frac{ds}{2\pi i} \int \frac{dk}{2\pi i} \frac{e^{st}\, e^{kx}}{k^2 + K^2(s)} \left\{ \left[\frac{\partial}{\partial \xi} \tilde{A}\right](\xi=0,s) + k\tilde{A}(\xi=0,s) \right.$$

$$\left. + \frac{a}{(\varepsilon_{xx}+is)(k + [|\varepsilon/\varepsilon_{xx}|]^{1/2})} \left[(\varepsilon+is) - \frac{\lambda^2}{[|\varepsilon|\ |\varepsilon_{xx}|]^{1/2}}\right] \right\} \tag{B.6}$$

where $\int$ refers to the appropriate Laplace inversion contours.

Equation (B-6) gives, in principle, the space-time evolution of the mode-conversion process provided the value of A and its spatial derivative are known at the edge. The simplest response contained in (B-6) is that due to a fixed amplitude at the boundary. Denoting this part of the solution as A_{II} yields

$$A_{II}(x,t) = \frac{a}{2} \int \frac{ds}{s} e^{st} \left[e^{iK(s)x} + e^{-iK(s)x}\right] \tag{B-7}$$

from which one obtains the asymptotic solutions ($t \to \infty$) corresponding to the mode-converted waves of the form

$$\exp\{\pm i[|\varepsilon\varepsilon_{zz}/\varepsilon_{xx}|]^{1/2}\ \xi\} \tag{B-8}$$

REFERENCES

1. T. H. Stix, Phys. Rev. Lett. 15, 878 (1965).
2. F. W. Perkins, R. L. Berger, and L. Chen, APS Bull. 20, 1313 (1975).
3. R. L. Berger, L. Chen, and F. W. Perkins, APS Bull. 20, 1314 (1975).
4. C. F. F. Karney and A. Bers, MIT Research Laboratory of Electronics QPR No. 116, 94 (1975).
5. P. K. Kaw, Princeton PPL Report Matt-1208 (1976).
6. G. J. Morales and Y. C. Lee, Phys. Rev. Lett. 35, 930 (1975).
7. W. Gekelman and R. L. Stenzel, Phys. Rev. Lett. 35, 1708 (1975).
8. B. Richards and R. R. Parker, APS Bull. 20, 1313 (1975).
9. W. M. Hooke, APS Bull. 20, 1313 (1975).
10. V. E. Golant, Zh. Tekh. Fiz. 41, 2492 (1971) [Sov. Phys. Tech. Phys. 16, 1980 (1972)].
11. R. R. Parker, MIT Research Laboratory of Electronics QPR No. 102, 97 (1971).
12. H. C. Kim, R. L. Stenzel, and A. Y. Wong, Phys. Rev. Lett. 33, 886 (1974).
13. G. J. Morales and Y. C. Lee, Phys. Rev. Lett. 33, 1016 (1974).
14. D. Potter, Computational Physics (Wiley, New York, 1973) p. 88.
15. Handbook of Mathematical Functions, edited by M. Abromowitz and I. A. Stegun (Dover, New York, 1970), p. 444.

FIGURE CAPTIONS

FIG. 1 Cartessian coordinate system and corresponding slab geometry used in the problem.

FIG. 2 Qualitative sketch indicating the direction of power flow associated with the evanescent radiation prior to mode-conversion.

FIG. 3 Spatial dependence of typical zero-order quantities investigated. The continuous curve represents the density profile, the dashed curve denotes the dielectric ε_{zz}, and the dotted curve corresponds to $|\underset{\sim}{E}|^2$ prior to mode-conversion.

FIG. 4 Spatial dependence of the real (continuous curve) and imaginary (dashed curve) parts of E_z for different times during the process of mode-conversion. Time interval displayed: a) $\upsilon t = 1.0$, b) $\upsilon t = 5.0$, c) $\upsilon t = 10.0$, d) $\upsilon t = 20.0$.

FIG. 5 Spatial penetration of RF energy into the plasma after mode-conversion takes place. Continuous curve is the density, dashed curve is the dielectric ε_{zz}. The dotted curve is $|E_z|^2$ at $\upsilon t = 20.0$, and should be compared with Fig. 3.

FIG. 6 Phasor plot of E_z at $\upsilon t = 5.0$. Parameter along curve is the spatial position into the plasma, and increases in the direction of the arrows. Clockwise rotation shows mode-converted wave is a backward wave.

FIG. 7 Phasor plot of E_x at $\upsilon t = 5.0$. Parameter along curve is the spatial position into the plasma, and increases in the direction of the arrows. Clockwise rotation shows mode-converted wave is a backward wave.

FIG. 8 Space-time penetration of RF energy in the linear regime over the time interval $0.5 \leq \upsilon t \leq 10.0$. Overlapping of curves for different times indicates approach to the steady-state.

FIG. 9 Typical nonlinear distortion of the density profile obtained for large external power levels. The continuous curve is the profile at $\upsilon t = 10.0$, and the dashed curve is the unperturbed profile.

FIG. 10 Nonlinear quenching of the mode-conversion process observed at large power levels. Shown are phasor plots of E_z for: a) linear case, and b) strong nonlinearity. Curves a) and b) are plotted on the same scale and correspond to equal times in the evolution.

FIG. 11 Nonlinear quenching of the mode-conversion process observed at large power levels. Shown are phasor plots of E_x for: a) linear case, and b) mild nonlinearity (compared to that used in Fig. 10). Curves a) and b) are on the same scale and correspond to equal times in the evolution.

FIG. 12 Time dependence of total electric field energy content in the plasma, U, for different values of the externally applied amplitude, E_o, in arbitrary units: linear case, $E_o = 1.0$, $E_o = 2.0$, $E_o = 3.0$.

FIG. 13 Dependence of the rate of electric field energy penetration into the plasma

$$\left[\overline{V} \equiv \frac{d}{dt}\left(\left|\int_{x_1}^{x_2} dx \left|\underset{\sim}{E}/E_o\right|^2\right|\right)\right]$$

on the externally applied power level, in arbitrary units. c is the speed of light. Heavy squares are numerical results, and solid curve is eyeball fit given by Eq. (58).

FIG. 14 Nonlinear space-time penetration of RF energy into the plasma over the interval $5.0 \leq \upsilon t \leq 10.0$. Dashed curved is the zero-order density profile; continuous curve next to dashed curve is the nonlinearly modified profile. To be compared with Fig. 8

FIG. 15 Spectacular nonlinear pulses and density striations observed at large power levels in shallow density profiles.

FIG. 16 Nonlinear propagation of multiple-peak pulse trains that give rise to intermittent transport of RF energy to the interior of the plasma. Behavior to be contrasted with linear result shown in Fig. 8.

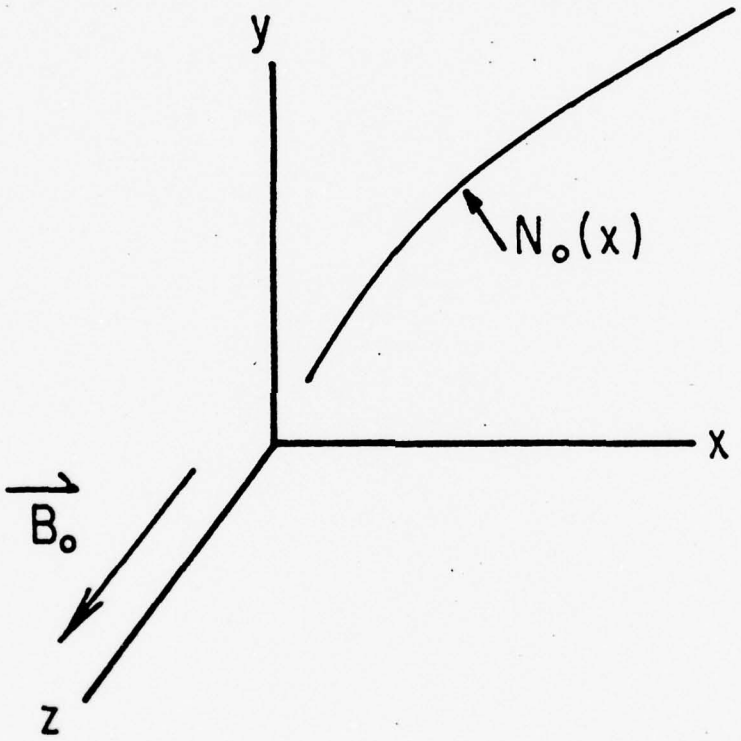

FIGURE 1

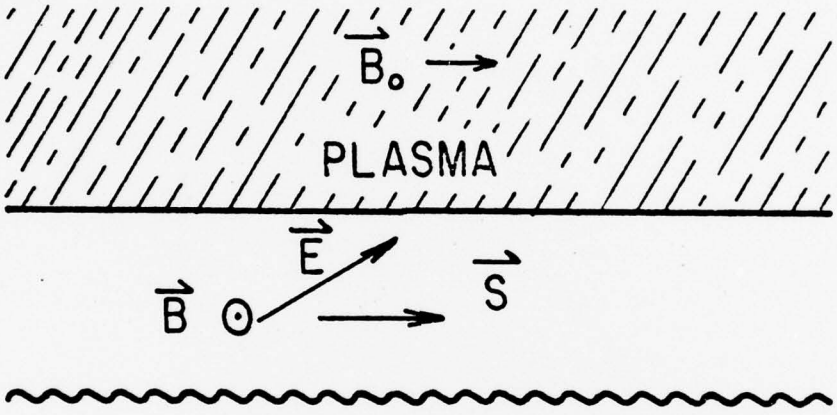

FIGURE 2

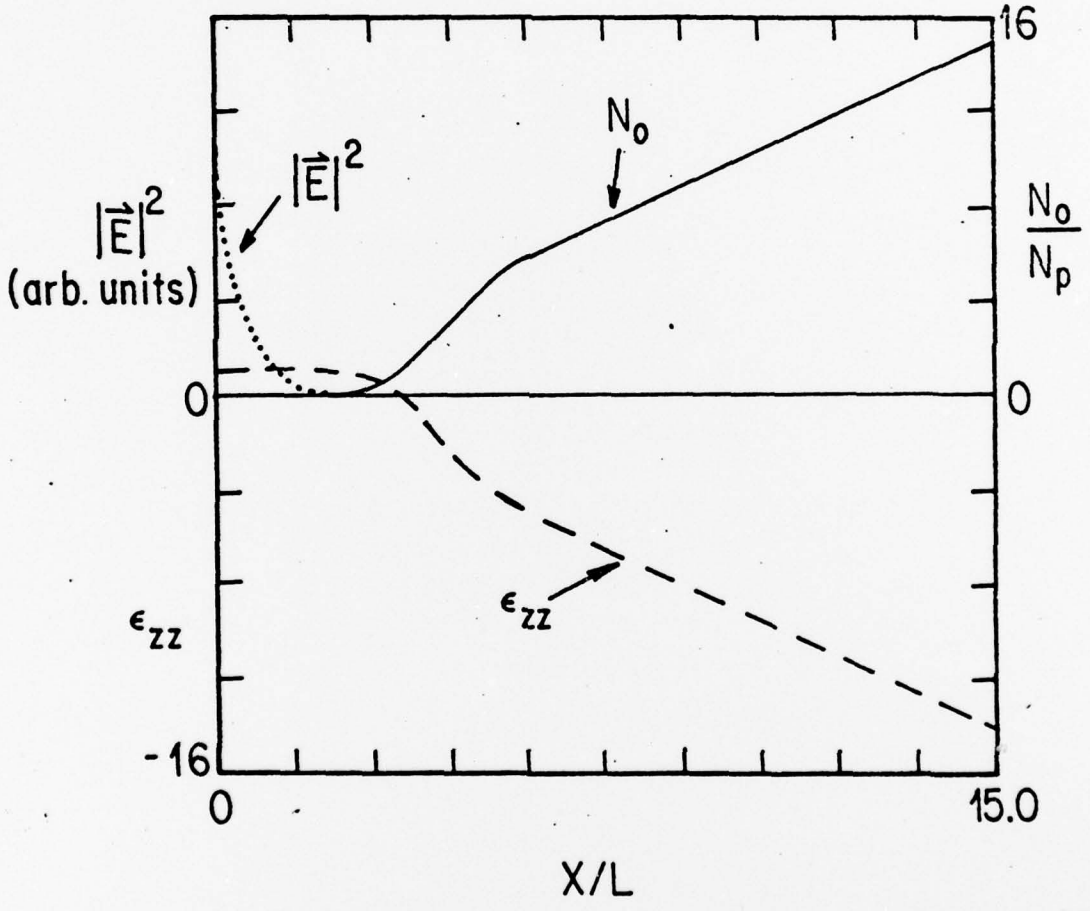
16
N_o
$|\vec{E}|^2$
$|\vec{E}|^2$
(arb. units)
$\frac{N_o}{N_p}$
0
0
ϵ_{zz}
ϵ_{zz}
-16
0
15.0
X/L

FIGURE 3

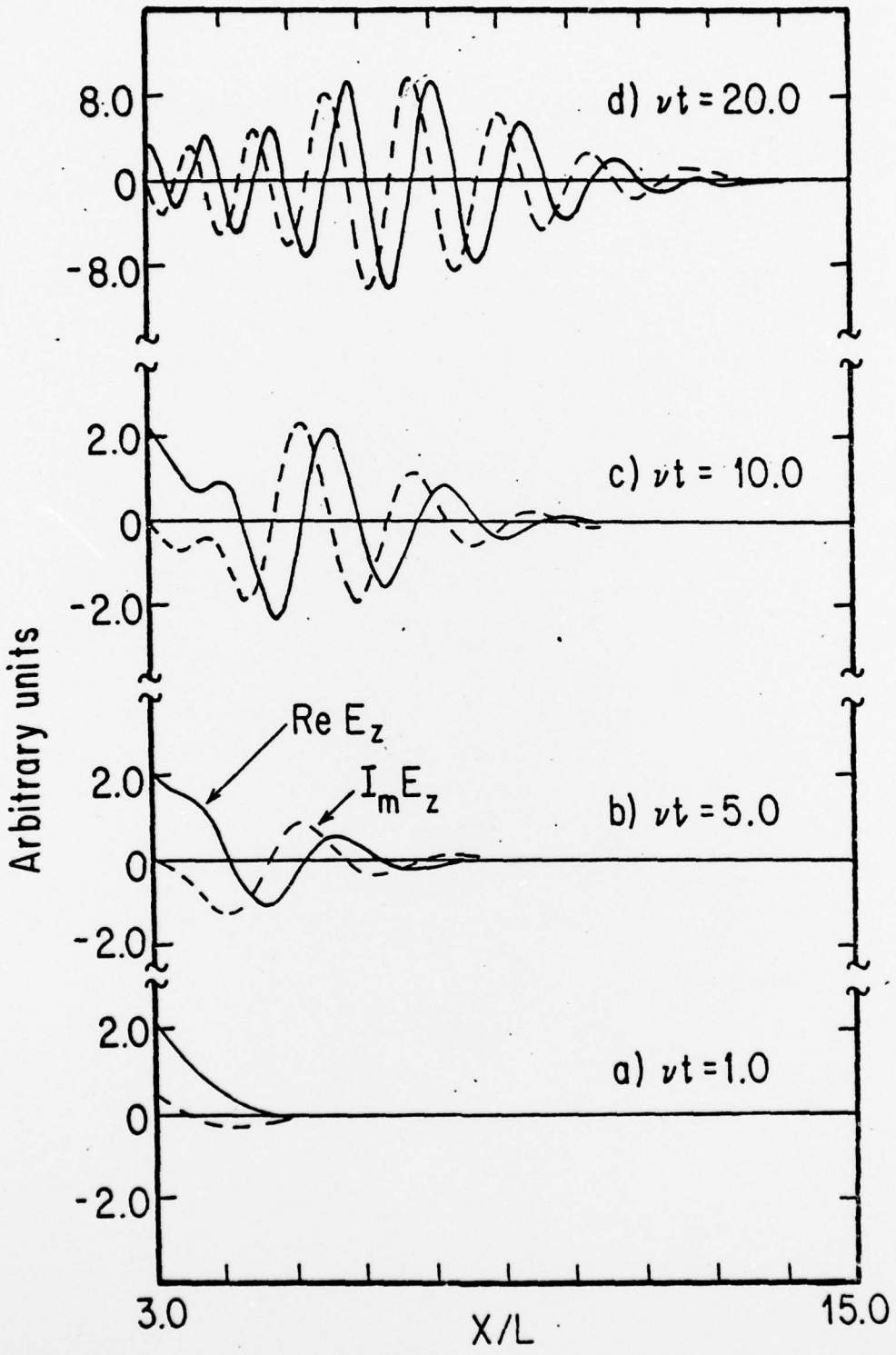
8.0
0
-8.0
d) νt = 20.0
2.0
0
-2.0
c) νt = 10.0
Re E_z
$I_m E_z$
2.0
0
-2.0
b) νt = 5.0
2.0
0
-2.0
a) νt = 1.0
Arbitrary units
3.0
X/L
15.0

FIGURE 4

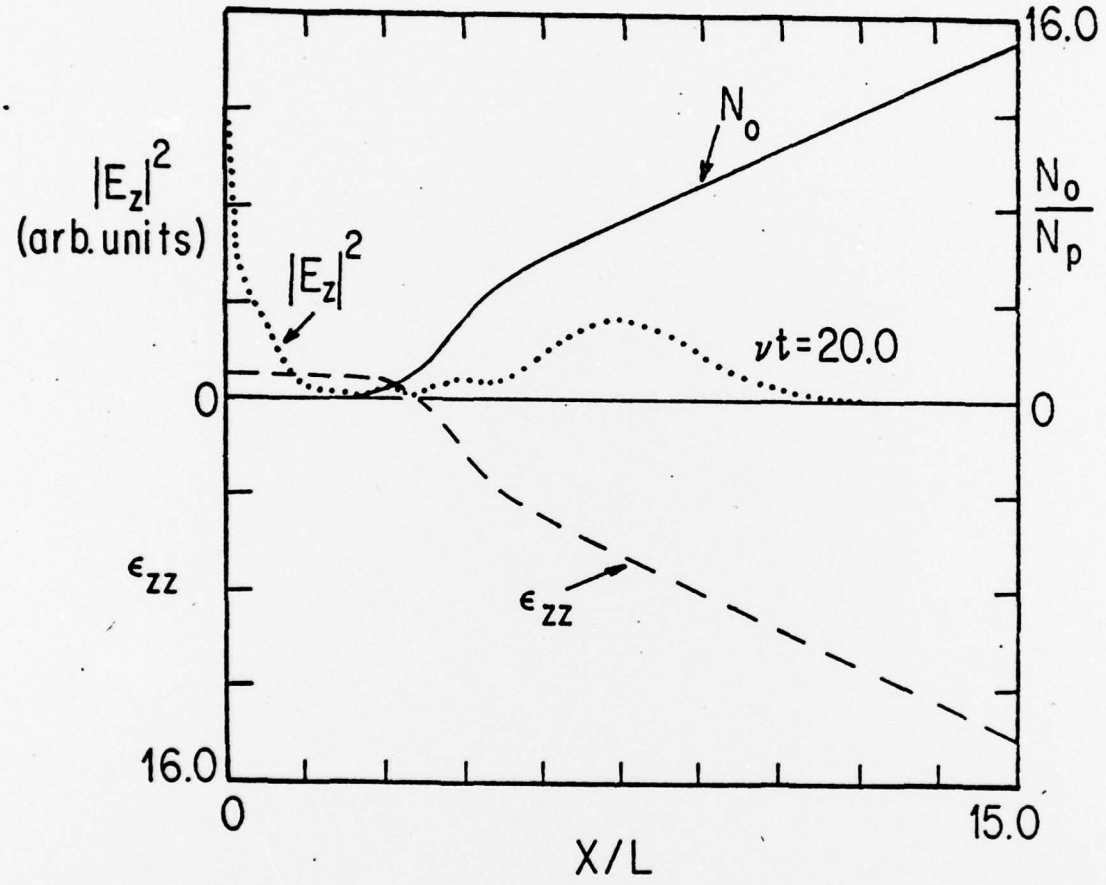
16.0
N_o
$|E_z|^2$
(arb. units)
$\frac{N_o}{N_p}$
$|E_z|^2$
$\nu t = 20.0$
0
0
ϵ_{zz}
ϵ_{zz}
16.0
0
15.0
X/L

FIGURE 5

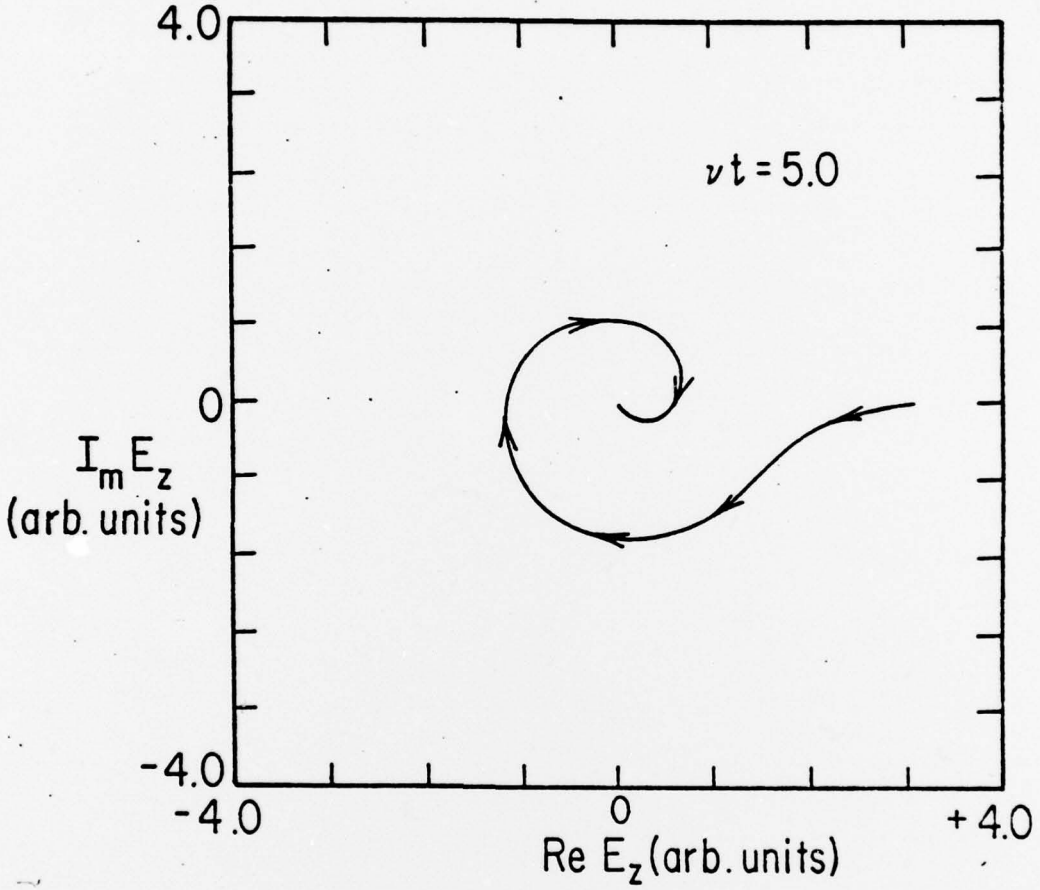

FIGURE 6

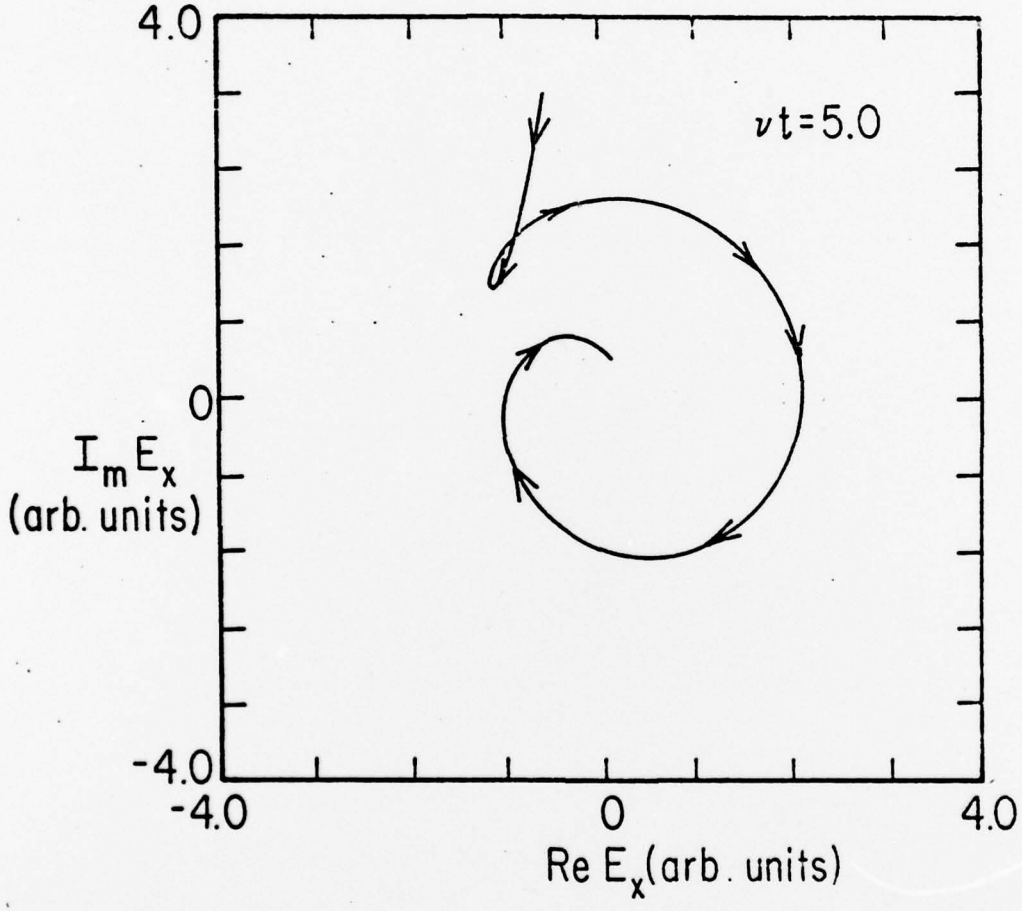

FIGURE 7

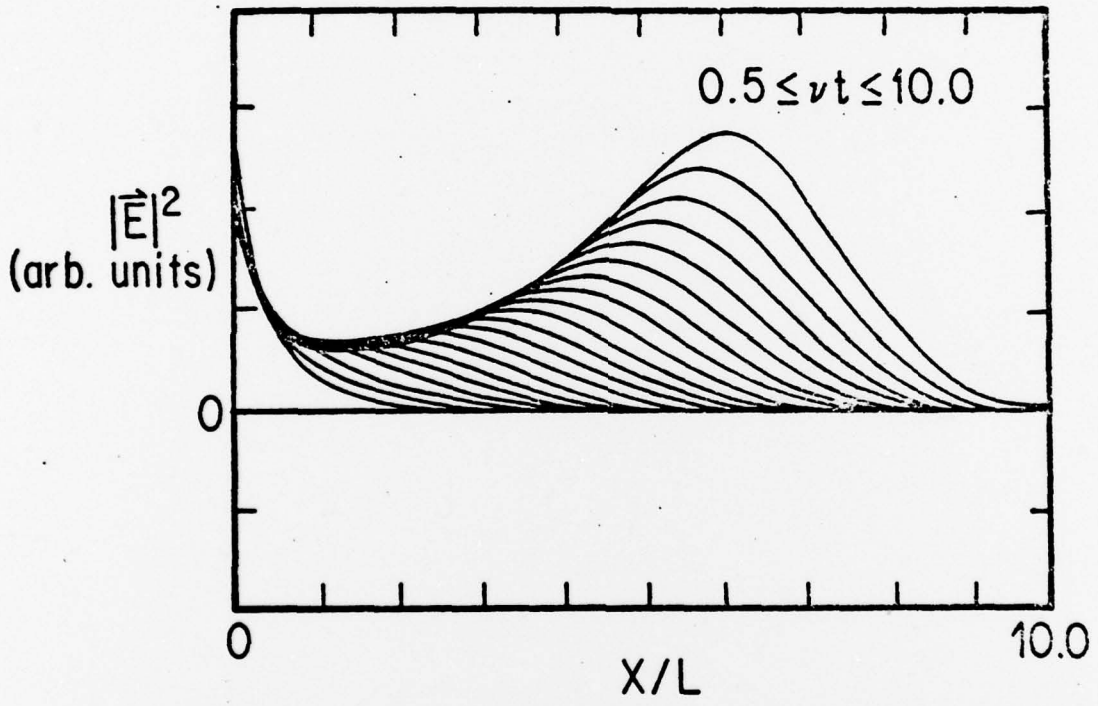

FIGURE 8

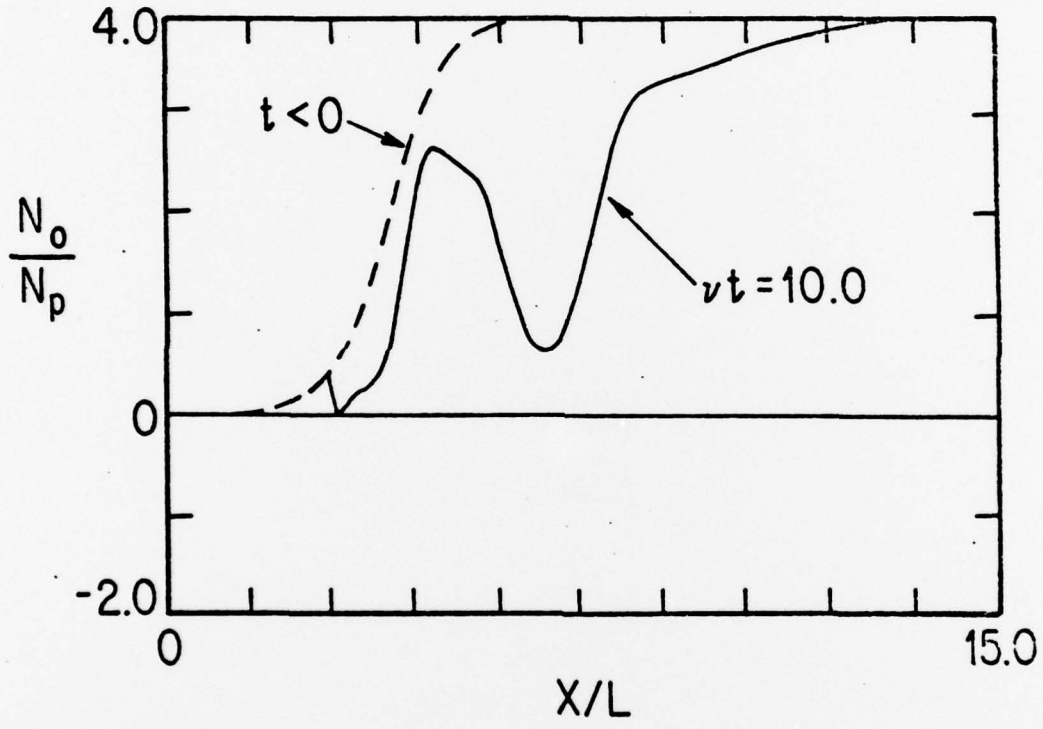

FIGURE 9

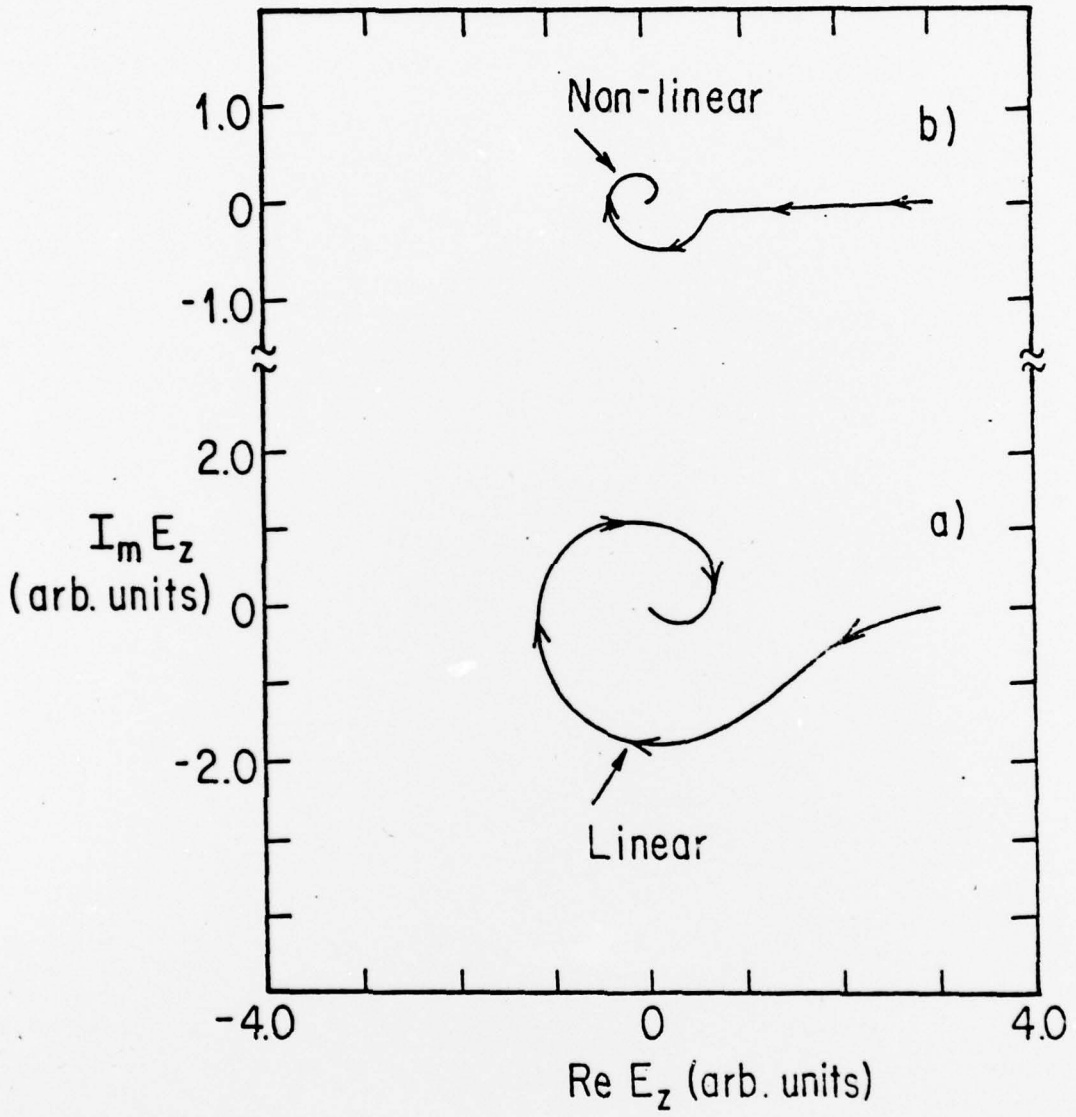
Non-linear
b)
1.0
0
-1.0
2.0
$I_m E_z$
(arb. units)
0
a)
-2.0
Linear
-4.0
0
4.0
Re E_z (arb. units)

FIGURE 10

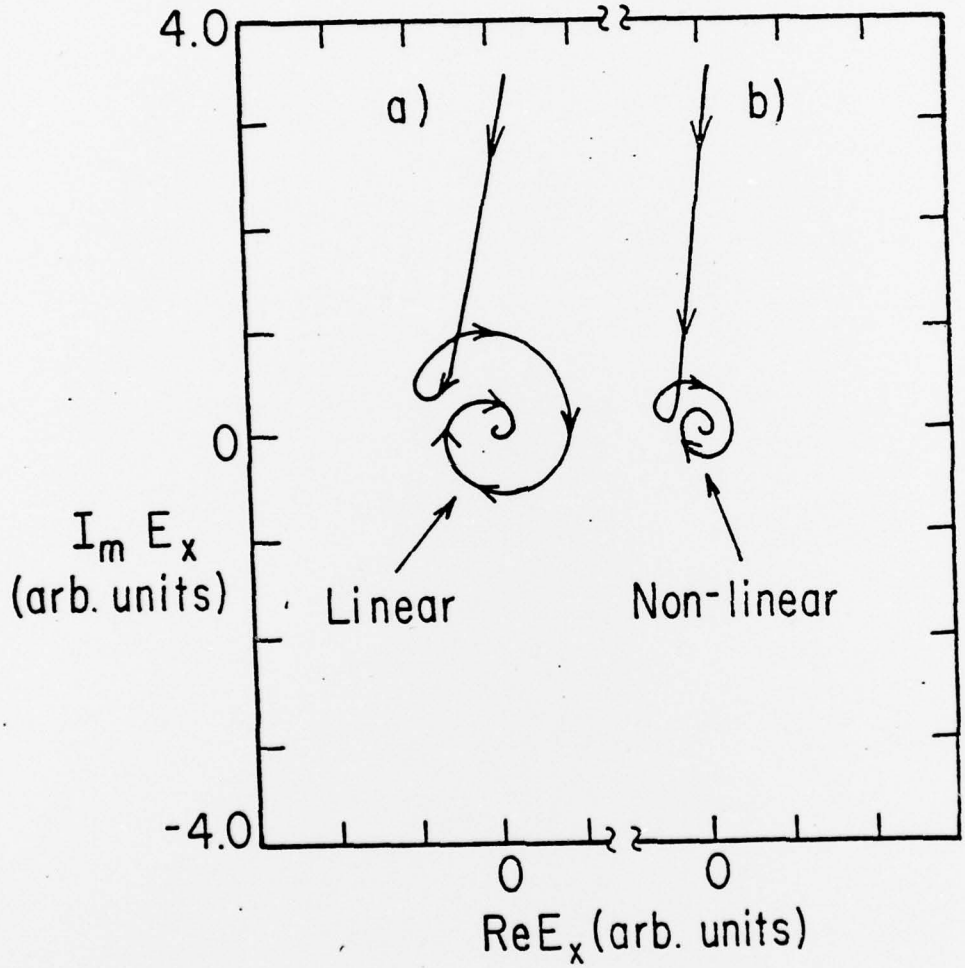

FIGURE 11

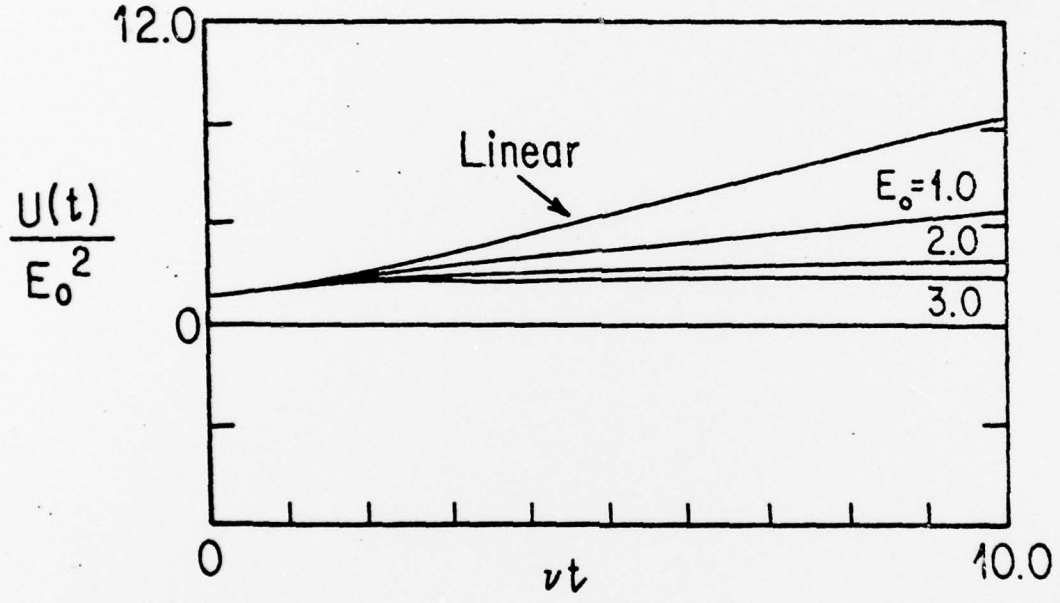

FIGURE 12

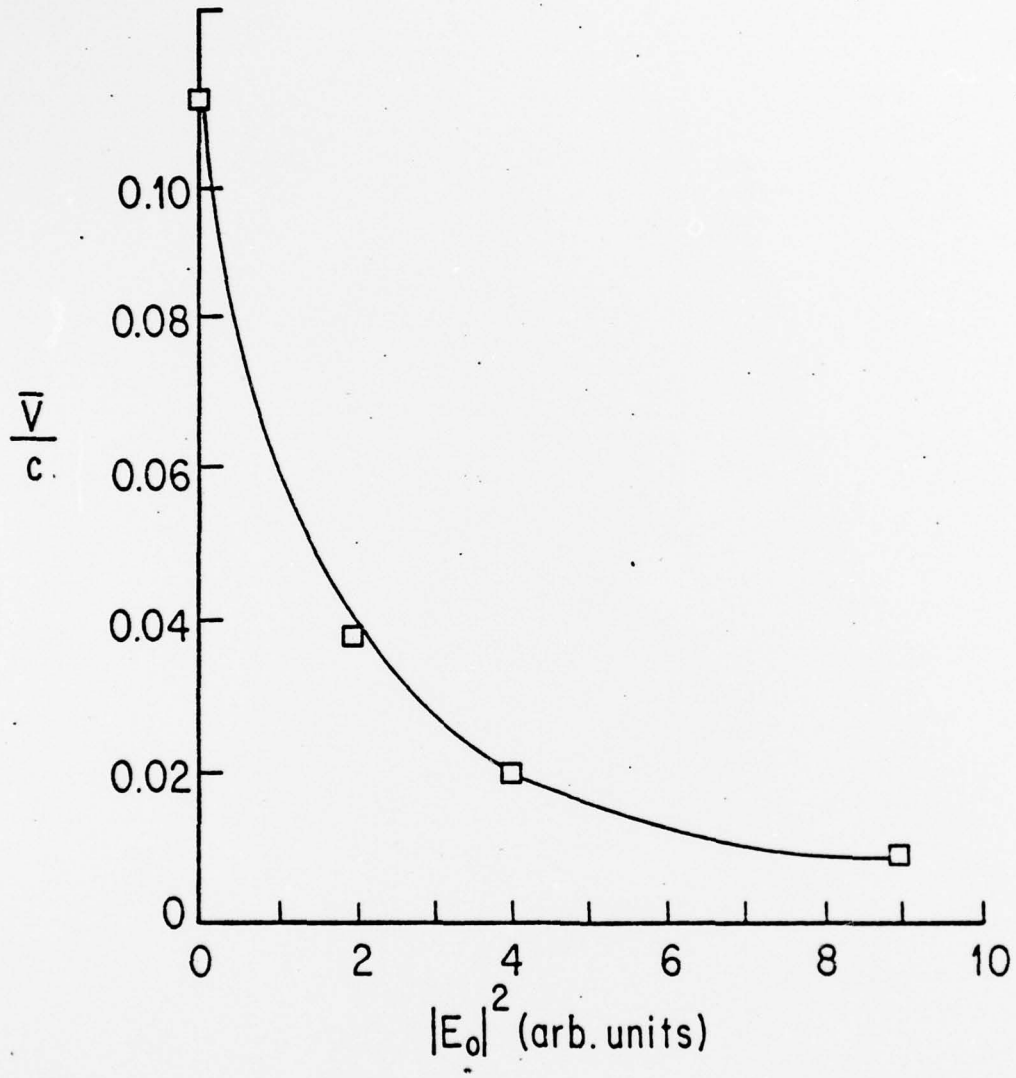

FIGURE 13

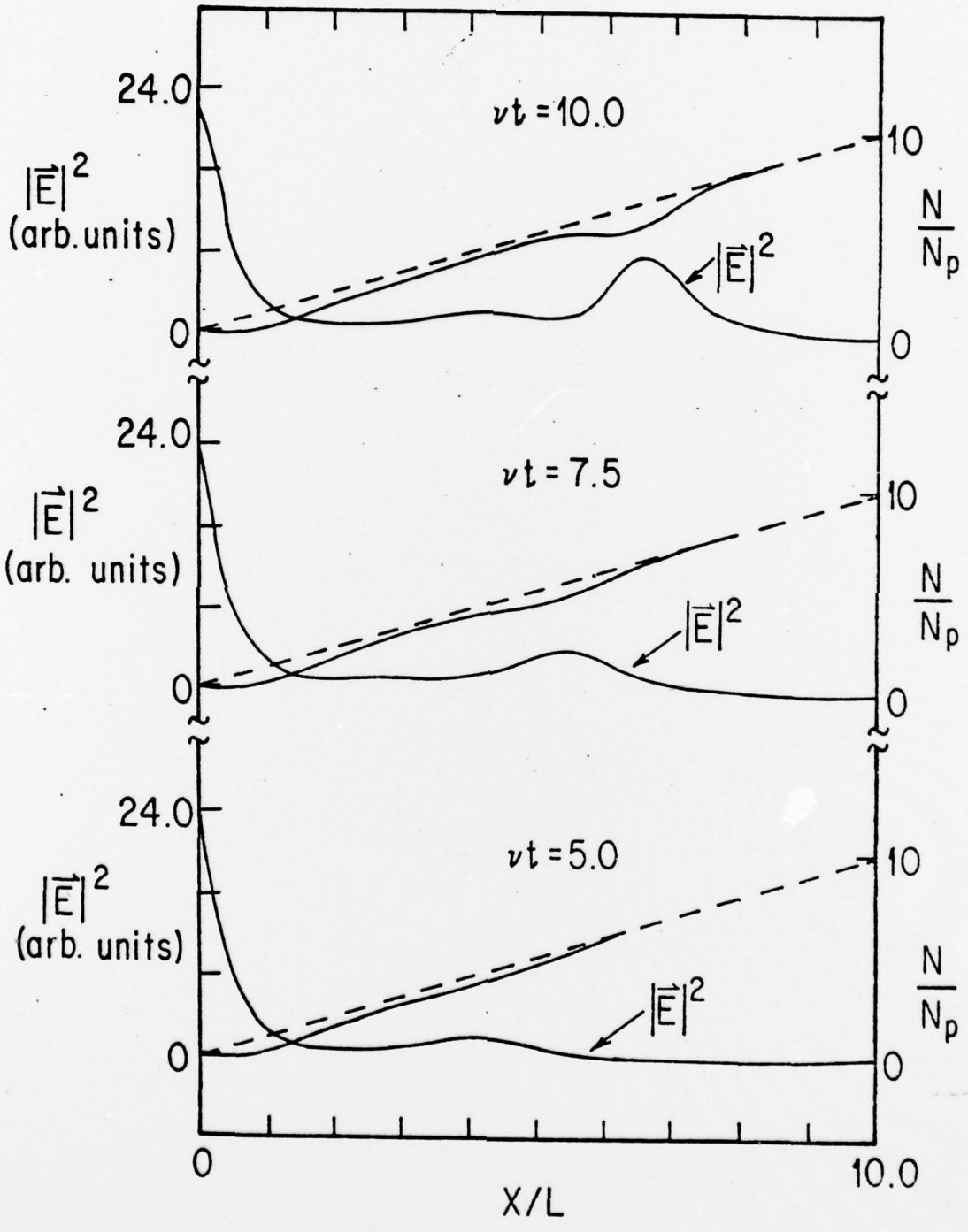
24.0
νt = 10.0
10
$|\vec{E}|^2$
(arb.units)
$|\vec{E}|^2$
$\frac{N}{N_p}$
0
0
24.0
νt = 7.5
10
$|\vec{E}|^2$
(arb. units)
$|\vec{E}|^2$
$\frac{N}{N_p}$
0
0
24.0
νt = 5.0
10
$|\vec{E}|^2$
(arb. units)
$|\vec{E}|^2$
$\frac{N}{N_p}$
0
0
0
10.0
X/L

FIGURE 14

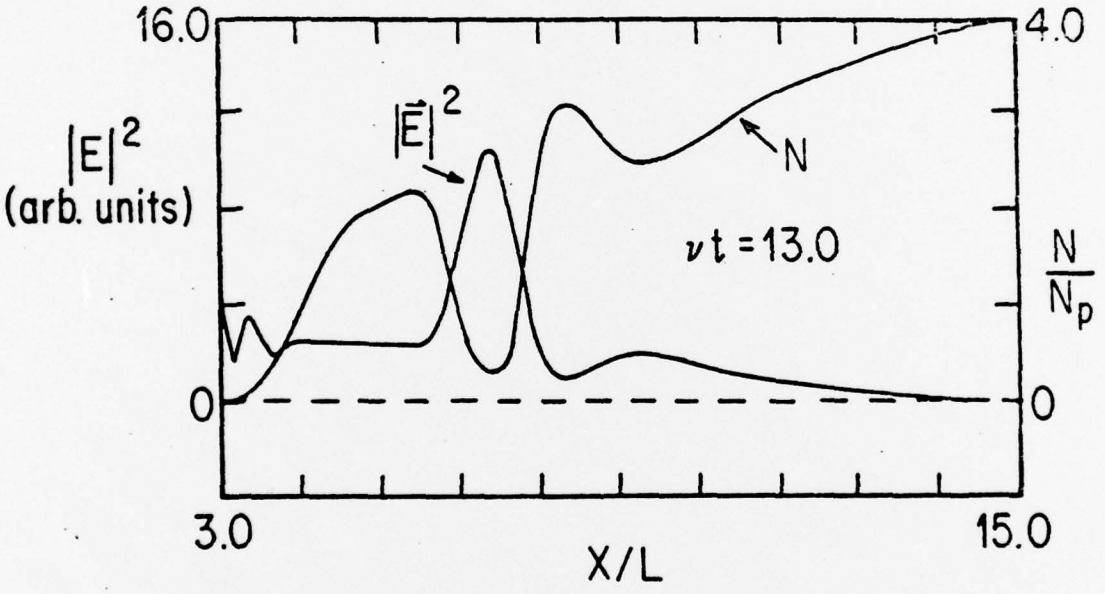

FIGURE 15

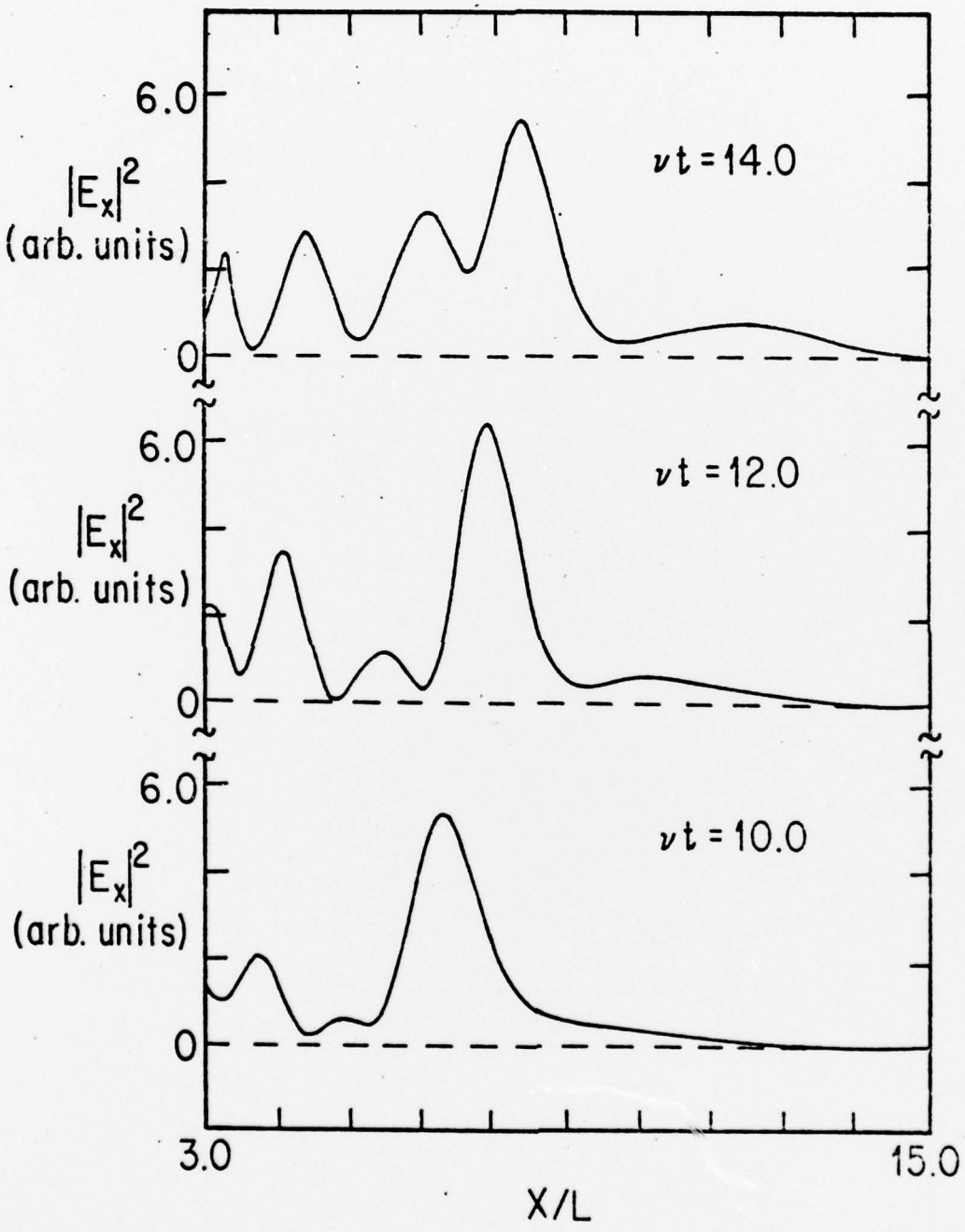
6.0
$|E_x|^2$
(arb. units)
0
$\nu t = 14.0$
6.0
$|E_x|^2$
(arb. units)
0
$\nu t = 12.0$
6.0
$|E_x|^2$
(arb. units)
0
$\nu t = 10.0$
3.0
15.0
X/L

FIGURE 16